Journal of Inflammation Research

Dovepress
Taylor & Francis Group

Open Access Full Text Article

ORIGINAL RESEARCH

A Pan-Cancer Analysis of Natriuretic Peptide Receptor 3 (NPR3) with Clinical Cohort and in vitro Validation

Yifan Liu[1,*], Jiangui Liu[1,*], Yuanan Li[1,*], Zihui Zhao[1,*], Donghao Lyu[1], Keqin Dong[1], Maodong Wei[1], Runzhi Huang[2], Bingnan Lu[1], Xiuwu Pan[1]

[1]Department of Urology, Xinhua Hospital Affiliated to Shanghai Jiao Tong University School of Medicine, Shanghai, 200092, People's Republic of China; [2]Department of Burn Surgery, the First Affiliated Hospital of Naval Medical University, Shanghai, 200433, People's Republic of China

*These authors contributed equally to this work

Correspondence: Xiuwu Pan; Bingnan Lu, Department of Urology, Xinhua Hospital Affiliated to Shanghai Jiao Tong University School of Medicine, No. 1665 Kongjiang Road, Shanghai, 200092, People's Republic of China, Email panxiuwu@126.com; 972081060@qq.com

Background: Natriuretic peptide receptor 3 (NPR3) regulates natriuretic peptides and plays a key role in angiogenesis, immune regulation, and progression of certain cancers. However, the clinical significance of NPR3 at pan-cancer level remains poorly understood. This study aimed to comprehensively analyze NPR3's role across multiple cancers, focusing on its potential as a prognostic biomarker, particularly in kidney cancer.

Methods: A comprehensive pan-cancer study of NPR3 was conducted using 20 different databases and datasets. The study included differential expression analysis, competing endogenous RNA (ceRNA) analysis, protein–protein interaction (PPI) analysis, Kaplan–Meier (K-M) survival analysis, and correlation assessments of NPR3 with clinical characteristics, tumor purity, tumor genomics, tumor immunity, drug sensitivity, molecular docking, and signaling pathways. Additionally, using a cohort of 370 patients diagnosed with kidney neoplasms, immunohistochemistry (IHC) was employed to assess NPR3 expression differences between tumor and normal tissues. The IHC cutoff point was determined using the "surv_cutpoint" function, followed by survival analysis. Multiple external datasets were used to validate the results. Cell-based experiments in 786-O, 769-P, and A-498 cell lines were further conducted.

Results: In pan-cancer, NPR3 was down-regulated in most of the tumor types, and ceRNA and PPI network were constructed. Moreover, NPR3 expression was significantly associated with the clinical prognosis and stages, tumor purity, genetic mutation, immune infiltration and signaling pathways and drug sensitivity. In kidney neoplasm, NPR3 was down-regulated, and higher expression was associated with a better prognosis. Multivariate Cox regression analysis showed that NPR3 expression was protective factor for both OS (HR = 0.50, 95% CI = 0.29–0.87, $p = 0.013$) and PFS (HR = 0.66, 95% CI = 0.46–0.95, $p = 0.024$). In renal cancer cells, NPR3-knockdown significantly suppressed tumor proliferative and migration activity.

Conclusion: NPR3 servers as a prognostic and immunotherapeutic biomarker in pan-cancer, but its biological role and potential as a therapeutic target warrants further investigation.

Keywords: NPR3, pan-cancer, kidney cancer

Introduction

Cancer has become a major global public health concern, imposing substantial socioeconomic burdens. In 2024, an estimated 2,001,140 new cancer cases occurred in the United States alone.[1] Despite the large number of patients requiring effective treatment, traditional therapies often fall short due to limited tumor specificity. Recently, tumor immunotherapy has shown great promise as a novel treatment approach.[2,3] However, the success of immunotherapy relies heavily on the identification of specific tumor biomarkers, which remain scarce for many cancer types.[4–6] Therefore, the discovery of novel biomarkers is essential for advancing precision oncology.

Received: 23 January 2025
Accepted: 11 July 2025
Published: 26 July 2025

Natriuretic peptide receptor 3 (NPR3) is a receptor for natriuretic peptides (NPs) and it functions as an antagonist in the renin-angiotensin-aldosterone system (RAAS). Unlike NPR1 and NPR2, which catalyze the synthesis of cGMP, NPR3 primarily acts by internalizing and degrading NPs through receptor-mediated mechanisms, thus removing them from circulation.[7,8] Additionally, NPR3 has been shown to either promote or inhibit the progression of various cancers,[9–15] with studies indicating that NPR3 plays a pivotal role in tumor growth and metastasis through its negative interaction with adenylyl cyclase and MAPK signaling pathways.[16,17]

Moreover, kidney cancer, especially kidney renal clear cell carcinoma (KIRC), is characterized by abnormal angiogenesis, metabolic reprogramming, and immune evasion.[18] The tumor microenvironment in KIRC is often infiltrated by various immune cells, including T cells, macrophages, and myeloid-derived suppressor cells, which play critical roles in tumor progression and response to immunotherapy.[19] Therefore, identifying biomarkers that reflect or influence this immune landscape is of high clinical relevance.[20] Although NPR3 has been scarcely investigated in kidney cancer, a previous study found that NPR3 may play a key role in the metastasis of KIRC.[21] However, while NPR3 has been previously linked to angiogenesis, immune regulation, and progression of multiple cancers, the prognostic significance of NPR3 at pan-cancer level, especially within kidney cancer, remains largely unexplored.

In this study, we conducted a comprehensive pan-cancer analysis of NPR3 by incorporating data from multiple databases to investigate its differential expression, ceRNA and PPI networks, clinical correlations, tumor purity, genomic alterations, immune infiltration and function, drug sensitivity, and associated signaling pathways. Furthermore, the bioinformatic results were validated in a cohort of 370 kidney neoplasm patients and in vitro experiments with kidney cancer cell lines.

Materials and Methods

Data Collection

The study was approved by the Ethics Committee of Xinhua Hospital Affiliated to Shanghai Jiao Tong University School of Medicine (XHEC-C-2021-145-1). Written informed consent to participate was obtained from all of the participants in the study. We collected the expression and clinical data for NPR3 across 33 tumor types from The Cancer Genome Atlas (TCGA) database.[22] A comprehensive list of the 33 tumor types and their abbreviations is provided in Table S1. Immunohistochemical (IHC) images of NPR3 expression in different tissues were obtained from Human Protein Atlas (HPA) database.[23] The NPR3 expression and clinical data for external validation was obtained from Clinical Proteomic Tumor Analysis Consortium (CPTAC) (PDC000127[24] and PDC000464[25]), GEO (Gene Expression Omnibus) (GSE22541,[26] GSE36895,[27] GSE53757,[28] GSE66272,[29] GSE126964,[30] and GSE167093[31]), and RCC_2020_Braun_Cohort.[32] MicroRNA (miRNA) data were sourced from several databases, including miRDB,[33] miRcode,[34] miRWalk,[35] DIANA-microT,[36] and the Encyclopedia of RNA Interactomes (ENCORI) database.[37] The miRNA-lncRNA interaction data were also retrieved from ENCORI. Protein-protein interaction (PPI) data were obtained from the STRING database.[38] Microsatellite instability (MSI) scores were provided by the study from Sameek Roychowdhury et al.[39] We utilized the cBioportal tool[40] and the Gene Set Cancer Analysis (GSCA) database[41] to perform gene alteration analysis. Immune cell infiltration data were accessed from TIMER 2.0[42] and the Tumor Immune Dysfunction and Exclusion (TIDE) database.[43] Drug sensitivity data were gathered from The Cancer Therapeutics Response Portal (CTRP),[44–46] the Genomics of Drug Sensitivity in Cancer (GDSC) database,[47–49] and the CellMiner database.[50,51] Signaling pathway data were sourced from the Kyoto Encyclopedia of Genes and Genomes (KEGG) database.[52] A retrospective cohort of 370 kidney neoplasm patients, who had surgery between 2016 and 2018, was established. Follow-up data were collected until March 2021. Tumor tissues and adjacent normal tissues were also gathered.

Differential Expression Analysis and IHC Images in Pan-Cancer

The R package "ggpubr" was used to explore the gene expression differences between tumor and normal tissues using the Wilcoxon test. Then the IHC images of NPR3 from HPA database were illustrated.

Competing Endogenous RNA (ceRNA) Network Construction in Pan-Cancer

We identified the potential miRNA that targeted NPR3 from miRDB, miRcode, miRWalk and DIANA-microT databases successively. Then the intersection of all potential miRNA was identified as key miRNA, based on which we explored the miRNA-lncRNA interaction in ENCORI databases. The association between key miRNA and NPR3 in pan-cancer was also verified through ENCORI databases.

Protein–Protein Interaction (PPI) Network Construction in Pan-Cancer

At the proteome level, possible interactions between NPR3 and other proteins were extracted from STRING database, and a PPI network was used to visualize them.

Clinical Relevance Analysis in Pan-Cancer

We used the median level of NPR3 expression to split patients into high-NPR3- and low-NPR3-expression groups. To assess the relationship between NPR3 expression and patient survival (overall survival [OS], disease-free survival [DFS], disease-specific survival [DSS], and progression-free survival [PFS]), Kaplan–Meier (K-M) survival analysis was employed. Univariate Cox regression analysis was conducted to calculate the hazard ratios (HR) for NPR3 expression across 33 tumor types, considering OS, DFS, PFS, and DSS. Forest plots were generated to visualize these results.[53] The relationship between clinical stages of the 33 tumor types and NPR3 expression was evaluated using the Wilcoxon test. Additionally, the correlation between NPR3 expression and bone metastasis was investigated, with boxplots used to display differential expression between primary tumors and bone metastases. For BRCA, five subtypes were classified according to the PAM50 method,[54] and the correlation between these subtypes and NPR3 expression was analyzed and visualized using boxplots.

ESTIMATE and CIBERSORT Analysis in Pan-Cancer

The microenvironment scores (immune scores and stromal scores) were calculated with the ESTIMATE algorithm.[55] A higher stromal score reflects an increased proportion of stromal components, while a higher immune score suggests greater infiltration of immune cells. As the abundance of immune and stromal cells increased, tumor purity was found to decrease. What's more, the CIBERSORT algorithm was utilized to estimate the proportion of immune cells in tumor tissues,[56] and their relationship with NPR3 expression was analyzed.

Genetic Alteration and Mutation Analysis in Pan-Cancer

We calculated the tumor mutational burden (TMB) across 33 tumor types using TCGA WES data.[57] Next, NPR3 gene alteration analysis was conducted using the cBioportal tool, drawing from data from ten pan-cancer studies,[58–67] and mutation data were visualized. Additionally, single nucleotide variation (SNV), copy number variation (CNV), and methylation mutation profiles of NPR3 were analyzed through the GSCA database, followed by survival analysis in patients with NPR3 mutations.

Immune Analysis in Pan-Cancer

A total of 47 immune related genes were introduced, and a co-expression heatmap was constructed, with the method of Spearman analysis, between the expression of immune genes and NPR3.

TIMER 2.0, which provides information on immune cell infiltration, was further utilized for immune infiltration estimation.[42] TIDE database was further explored for CTL data.[43] Based on multiple data sources,[22,68,69] correlation curves were drawn between the expression of NPR3 and CTL. K-M curves were generated to examine the impact of NPR3 on CTL exclusion and dysfunction across these groups.

Drug Sensitivity Prediction in Pan-Cancer

The half maximal inhibitory concentration (IC50) values of drugs and the corresponding NPR3 mRNA expression levels from the GDSC, CTRP, and CellMiner databases. The IC50 values of drugs were analyzed from the CTRP and GDSC

databases. While, from the CellMiner database, the *Z* scores of certain drugs were analyzed, with higher *Z* scores indicating increased drug sensitivity.

Molecular docking analysis was conducted with the help of PyMOL (v1.3, Schrödinger, LLC) to eliminate water molecules and incorporate hydrogen atoms into the 3D structure of DPP4. PDBQT files for the receptors and ligands were generated with AutoDock Tools,[70] which also enabled the configuration of a 3D grid box around the receptor's binding site. Following this, AutoDock Vina was employed to predict the optimal binding conformations of the ligands to the receptors, with the results subsequently analyzed in PyMOL.[71]

Gene Set Enrichment Analysis of NPR3 in Pan-Cancer

The "clusterProfiler" R package helped us to find out the most enriched pathways in different cancer types.[72] The pan-cancer data were split into high-NPR3- and low-NPR3-expression subgroups, which were then reordered according to the fold change of differential expression. Then the gene expression profiles of each sample were compared with those of specific pathways, and the top five pathways with p-values < 0.05 in each tumor type were visualized.

Immunohistochemical (IHC) Staining and Scoring

The tissue samples from tumor and adjacent normal areas of 370 kidney neoplasm patients were initially preserved, paraffin-embedded, and sliced. Following this, the slices underwent a process of removal of paraffin and rehydration, after which NPR3 antigens were exposed through retrieval using a citrate buffer (pH = 6.0). Subsequently, the samples were treated with 3% hydrogen peroxide solution to block endogenous peroxidase activity, and then rinsed with PBS. To avoid non-specific binding, the tissues were treated with a 3% bovine serum albumin (BSA) solution. Primary antibodies against NPR3 (1:100; Proteintech; 26706-1-AP) were applied. Then the secondary antibodies conjugated to horseradish peroxidase (HRP) were subsequently applied. The HRP activity was visualized using diaminobenzidine (DAB), which produces a color reaction in the presence of NPR3. Hematoxylin was used for counterstaining to highlight the nuclei. The tissue slides were then dehydrated with solutions containing alcohol. Light microscope was used to examine samples. Two pathologists, experienced in this field, assessed the slides, and any discrepancies were resolved by a third pathologist. The IHC scoring criteria were based on the H-score system: H-score = $\sum$(pi×i) = (percentage of weak intensity*100) + (percentage of moderate intensity*200) + (percentage of strong intensity*300),[73] yielding a score that ranged from 0 to 300.

Clinical Analysis of NPR3 in Kidney Neoplasm

Clinical data were collected from 370 kidney neoplasm patients. With the help of "surv_cutpoint" in R, the optimal cutoff value for the IHC score was explored for OS and progression-free survival (PFS) separately. All patients were divided into high- and low-NPR3 expression group, and K-M survival curves were constructed. Subsequently, we treated NPR3 expression as a continuous variable and performed both univariate and multivariate Cox regression analyses for OS and PFS to evaluate its prognostic significance. Deviance residual plots were used to evaluate model fit and identify potential outliers. To assess the model's performance, calibration curves and receiver operating characteristic (ROC) curves were generated. Based on the multivariate model, risk scores were calculated for each individual, and patients were stratified into high-risk and low-risk groups according to the median risk score. Scatter plots and K-M survival curves were then used to compare survival outcomes between the two groups. In addition, nomograms were developed to predict individual survival probabilities at 1, 2, 3, 4, and 5 years.

External Validation for Kidney Neoplasm Patients

External expression and clinical data were extracted from CTPAC database, GEO database, and RCC_2020_Braun_Cohort. The gene expression differences between tumor and normal tissues using the Wilcoxon test. K-M survival curves were conducted to compare survival outcomes between high- and low-NPR3 groups.

Cell Experiments of NPR3 in 786-O, A-498, and 769-P Cells

The cell-line 786-O, A-498, 769-P (human renal cancer cells) was obtained from the American Type Culture Collection (ATCC). Three shRNAs were designed and one of them was proved to effectively knockdown NPR3 in 786-O, A-498

and 769-P cells. The shRNA sequence was CCAGGAGGTTATTGGTGATTA. It was delivered into cells by hU6-MCS-CBh-gcGFP-IRES-puromycin vector (GENECHEM). The control sequence was TTCTCCGAACGTGTCACGT. The primer designed for NPR3 qPCR was:

Forward Primer AGACTACGCCTTCTTCAACATTG

Reverse Primer GCTTCAAAGTCGTGTTTGTCTCC

The cells were infected with NPR3 shRNA or control shRNA viral particles, using 5 μg/mL of HiTransG A (GENECHEM, Shanghai, China) for 48 hours. Following infection, stable clones were isolated using 2 μg/mL puromycin for one week. The knockdown efficiency of NPR3 was verified through quantitative real-time PCR (qPCR) and Western Blot (WB), using primers and NPR3 specific antibody at 1:2000 dilution (#26,706-1-AP, Proteintech, IL, USA).

For the cell proliferation test, NPR3-knockdown 786-O, A-498 and 769-O cells were plated at a density of 1,000 cells per well in 96-well plates. After 1 hour of incubation with 10% CCK-8 solution, optical density was measured at 450 nm at 0, 24, 48, 72 and 96 hours to monitor cell growth. In the clone formation assay, 300 NPR3 knockdown and controlled cells were seeded in 6-well plates and waited for 10 days to stain and count. In the Transwell migration and invasion assays, 10,000 controlled and NPR3 knockdown cells were seeded onto upper chambers of Transwell inserts, each containing 100 μL serum-free RMPI 1640 medium (#11875093, Thermo Fisher Scientific). For assessing invasion capability, upper inserts were precoated with Matrigel at a 1:20 dilution (BD Biosciences, San Jose, CA, USA). Lower compartments contained RMPI 1640 medium supplemented with 10% fetal bovine serum (FBS) to promote cellular migration. After incubation for 24 hours, migrated or invaded cells were collected, fixed using paraformaldehyde, stained utilizing hematoxylin, and quantified via ImageJ software (https://imagej.net/ij/, NIH, USA).

In the scratch assay, both NPR3-knockdown and control cells were cultured at 1×10^6 cells per well in 6-well plates. After 24 hours, when a monolayer had formed, a straight scratch was made with the help of a 20 μL pipette tip. Images were captured at time points 0 and 24 hours, and the healing rate was assessed using ImageJ (NIH, USA).

To explore how dasatinib influences NPR3 levels, CCK-8 tests were used to ascertain the dasatinib IC50 values for cell lines 786-O, A498, and 769P. Initially, 1000 cells were distributed per well into 96-well plates. Dasatinib was subsequently administered at concentrations of 100 μM, 20 μM, 4 μM, 0.8 μM, 0.16 μM, and 0.032 μM after 24 hours. Following next 24 hours, proliferation was evaluated by measuring optical density at 450 nm. Dose–response curves were plotted, and IC50 values were computed using GraphPad Prism software. Next, cell cultures were split into two groups: one group received treatment with dasatinib at the IC50 concentration, while the control group was exposed to an equivalent DMSO volume. Cells underwent collection after 24-hour incubation for further qPCR. Relative mRNA expression was determined via the 2-ΔΔCq method and normalized against actin gene and the control sample, with each well containing 90 μL medium plus 10 μL CCK-8 reagent.

Statistical Analysis

R version 4.3.2 software was utilized for statistical analysis. For continuous variables that were normally distributed and had homogeneous variances, a Student's *t*-test was employed. If these conditions were not met, the Wilcoxon test was utilized instead. For categorical variables, the Chi-square test was employed. Statistical significance was determined with a threshold of $p < 0.05$ (two-tailed) and a false discovery rate (FDR) of less than 0.05.

Results

Transcriptome and Proteome Analysis of NPR3 in Pan-Cancer

The analysis flow chart was shown in Figures 1A and S1. The result of the differential expression analysis of NPR3 gene is displayed in Figure 1B. The results indicated that NPR3 was down-regulated, at the transcriptome level, in multiple tumor types, including BLCA, BRCA, COAD, HNSC, KICH, KIRP, LIHC, LUAD, LUSC, READ, STAD, THCA, UCEC, and UCS. To further understand the regulatory mechanisms underlying NPR3's downregulation, we explored potential miRNA interactions and constructed a ceRNA network. We intersected the target miRNA to NPR3 from miRDB, miRcode, miRWalk and DIANA-microT databases, and identified key miRNAs (Figure S2A). We further verified that, in pan-cancer, NPR3 expression was significantly related with the expression level of 23 key miRNAs

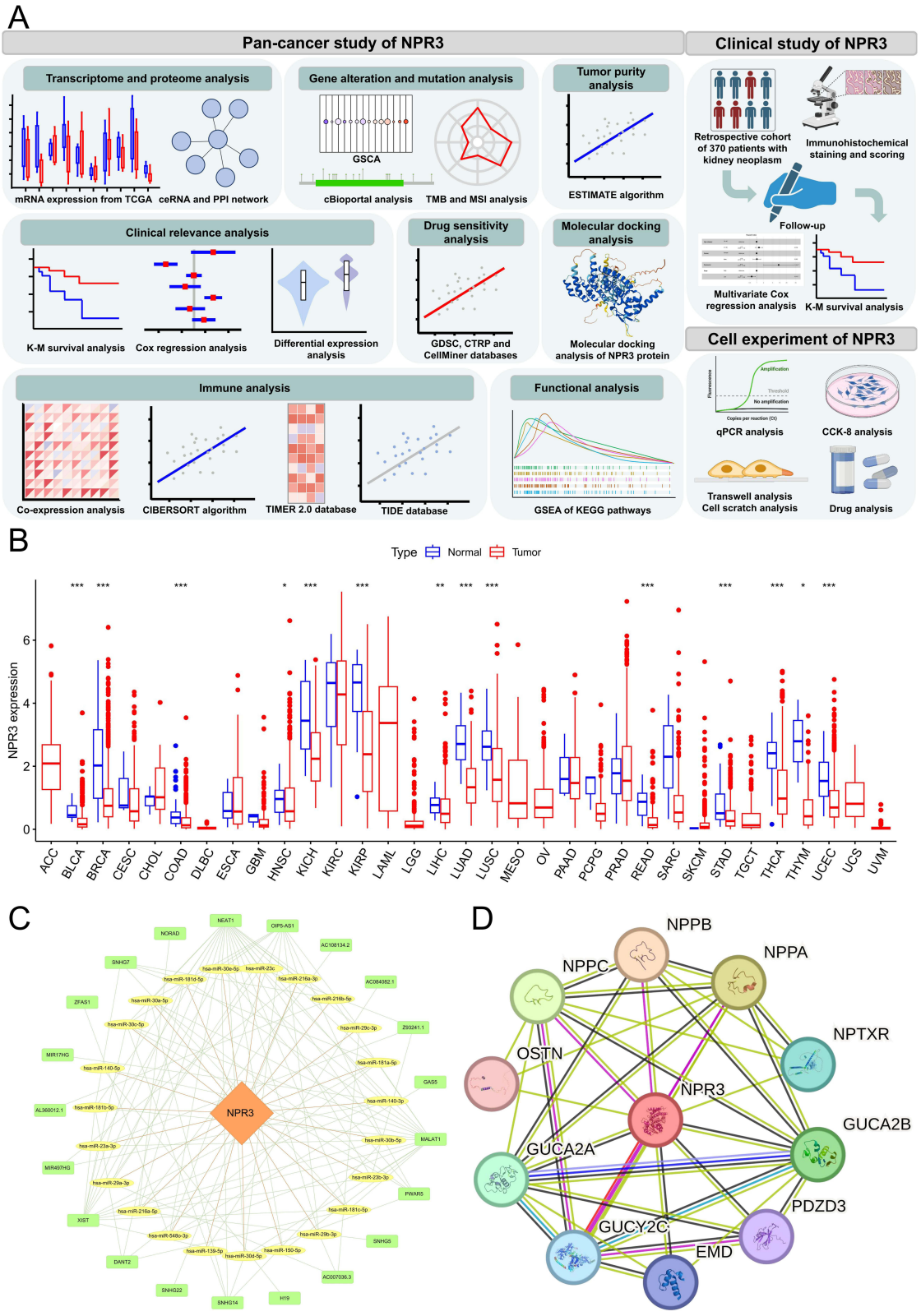

Figure 1 The flow chart, differential expression analysis, ceRNA network construction, and PPI network construction. (**A**) The flow chart of our analysis. (**B**) Expression of NPR3 in 33 tumor types between normal tissues and tumor tissues. NPR3 showed low expression in BLCA ($p < 0.001$), BRCA ($p < 0.001$), COAD ($p < 0.001$), HNSC ($p < 0.05$), KICH ($p < 0.001$), KIRP ($p < 0.001$), LIHC ($p < 0.01$), LUAD ($p < 0.001$), LUSC ($p < 0.001$), READ ($p < 0.001$), STAD ($p < 0.001$), THCA ($p < 0.001$), UCEC ($p < 0.05$) and UCS ($p < 0.001$). (**C**) The ceRNA network of NPR3. There were 23 miRNAs correlated with NPR3 and there were 21 lncRNAs correlated with miRNAs above. (**D**) The PPI network of NPR3. At the proteomic level, NPR3 was closely associated with NPTXR, NPPB, NPPA, NPPC, OSTN, GUCA2B, GUCA2A, GUCY2C, PDZD3 and EMD.

Abbreviations: IHC, Immunohistochemical; TMB, Tumor mutation burden; MSI, Microsatellite instability; ceRNA, competing endogenous RNA; lncRNA, long non-coding RNA; PPI, Protein–protein interaction; K-M, Kaplan-Meier; CCK-8, Cell counting kit-8; qPCR, quantitative real-time polymerase-chain reaction.

(Figure S2B). Then, we retrieved the lncRNA that were targeted by all the miRNA mentioned above, and a ceRNA network was constructed (Figures 1C and S2C). After that, the protein–protein interaction of NPR3 was investigated. At the proteome level, NPR3 showed close associations with NPTXR, NPPA, NPPB, NPPC, OSTN, GUCA2B, GUCA2A, GUCY2C, PDZD3, and EMD (Figure 1D). Moreover, IHC images showed that NPR3 expressed less in tumor tissues than in normal kidney and endometrium (Figure S3).

Clinical Relevance Analysis of NPR3 in Pan-Cancer

We conducted the survival analysis to evaluate patients' prognosis. K-M survival curves unveiled that high NPR3 expression was correlated with shortened OS in GBM, while it was correlated with longer OS in ACC and KIRC (Figure 2A). As for DFS, it was shown that higher NPR3 was correlated with longer DFS in LGG and THCA, while it was correlated with shortened DFS in STAD (Figure S4A). Similarly, in the aspect of DSS, it was implied that the higher NPR3 was associated with longer DSS in ACC, KIRC, KIRP, and LUSC, whereas it was associated with shortened DSS in GBM and STAD (Figure S4B). For PFS, it was indicated that higher NPR3 expression was correlated with longer PFS in KIRC and THCA, while it was associated with shortened PFS in COAD, DLBC and STAD (Figure S4C).

Furthermore, univariate Cox regression models were constructed in OS, DFS, DSS, and PFS, respectively. The results showed that, when it came to OS, NPR3 expression posed risk in BLCA, BRCA, KICH, SARC, and STAD, and it was favorable in ACC, KIRC, and KIRP (Figure 2B). As for DFS, NPR3 expression posed risk in STAD, while it was favorable in LUAD (Figure 2C). For DSS, NPR3 expression posed risk in STAD, BRCA, and BLCA, while it was favorable in KIRC, ACC, and KIRP (Figure 2D). For PFS, NPR3 expression posed risk in STAD, BLCA, and LGG, while it was favorable in KIRC, SKCM, and ACC (Figure 2E).

Clinical stages were also examined. Higher NPR3 showed a more advanced clinical stage in COAD and READ, while it was negatively correlated with KIRC and THCA (Figure S5A). In BLCA, BRCA, MESO, and PRAD, no significant association between NPR3 expression and bone metastasis was discovered (Figure S5B). However, a significant link was shown between NPR3 expression and the molecular subtypes of BRCA (Figure S5C).

Tumor Purity Analysis and Genetic Mutation Analysis of NPR3 in Pan-Cancer

We then used ESTIMATE algorithm to calculate stromal scores and immune scores, and their correlation with NPR3 expression was shown. In the aspect of immune scores, higher NPR3 was correlated with higher ones in BLCA, BRCA, COAD, LUAD, and PCPG, but it was correlated with lower ones in GBM, HNSC, TGCT, THCA, and THYM (Figures 3A and S6A). For stromal scores, higher expression of NPR3 was correlated with higher ones in almost all tumor types (Figures 3B and S6B).

Then, we the association between NPR3 expression and TMB and MSI were analyzed. As for TMB, Spearman correlation analysis showed a negative correlation in the majority of cancer types. Conversely, a positive correlation was observed in THYM and LGG. (Figure 3C). When it comes to MSI, a negative correlation was observed in CHOL, ESCA, PCPG, SKCM, STAD, and UCS, while a positive correlation was observed in MESO (Figure 3D).

Then the cBioportal was utilized to explore the main mutation sites of NPR3 gene. Among all tumors, 121 variants of uncertain significance (VUS) were identified in total, which included 102 missense, 11 truncating, 6 splice, 1 inframe, and 1 fusion (Figure S7A). GSCA revealed that the main SNV class of NPR3 was C>T (Figure S7B), and the there was a significant difference between mutant and wild-type NPR3 in PFS and DFS of BRCA patients (Figure S7C). Regarding CNV, the positive correlation between CNV and mRNA expression of NPR3 was significant in SARC, HNSC, and ESCA (Figure S7D). In comparison to homozygous CNVs, heterozygous CNVs of NPR3 accounted for a higher proportion in most tumor types (Figure S7E). The survival difference between CNV and wide type indicated that the CNV showed a significant correlation with patient survival (OS, DSS, DFS, PFS) in different cancer types (Figure S7F). Besides, methylation showed negative correlation with mRNA expression of NPR3 in all tumor types except for DLBC and PAAD (Figure S7G), while methylation was significantly up-regulated in tumor tissues in BRCA, LUAD, LUSC, PRAD, COAD, BLCA, UCEC, HNSC, KIRP, and THCA (Figure S7H). Methylation was correlated with longer DFS in BRCA, and longer OS in LIHC. However, it was correlated with shortened PFS in KIRP, of DSS in LGG, GBM, KIRP, KIRC, and ACC, and shortened OS in KIRC and ACC, for PFS in SKCM, CHOL, KIRC, and ACC (Figure S7I).

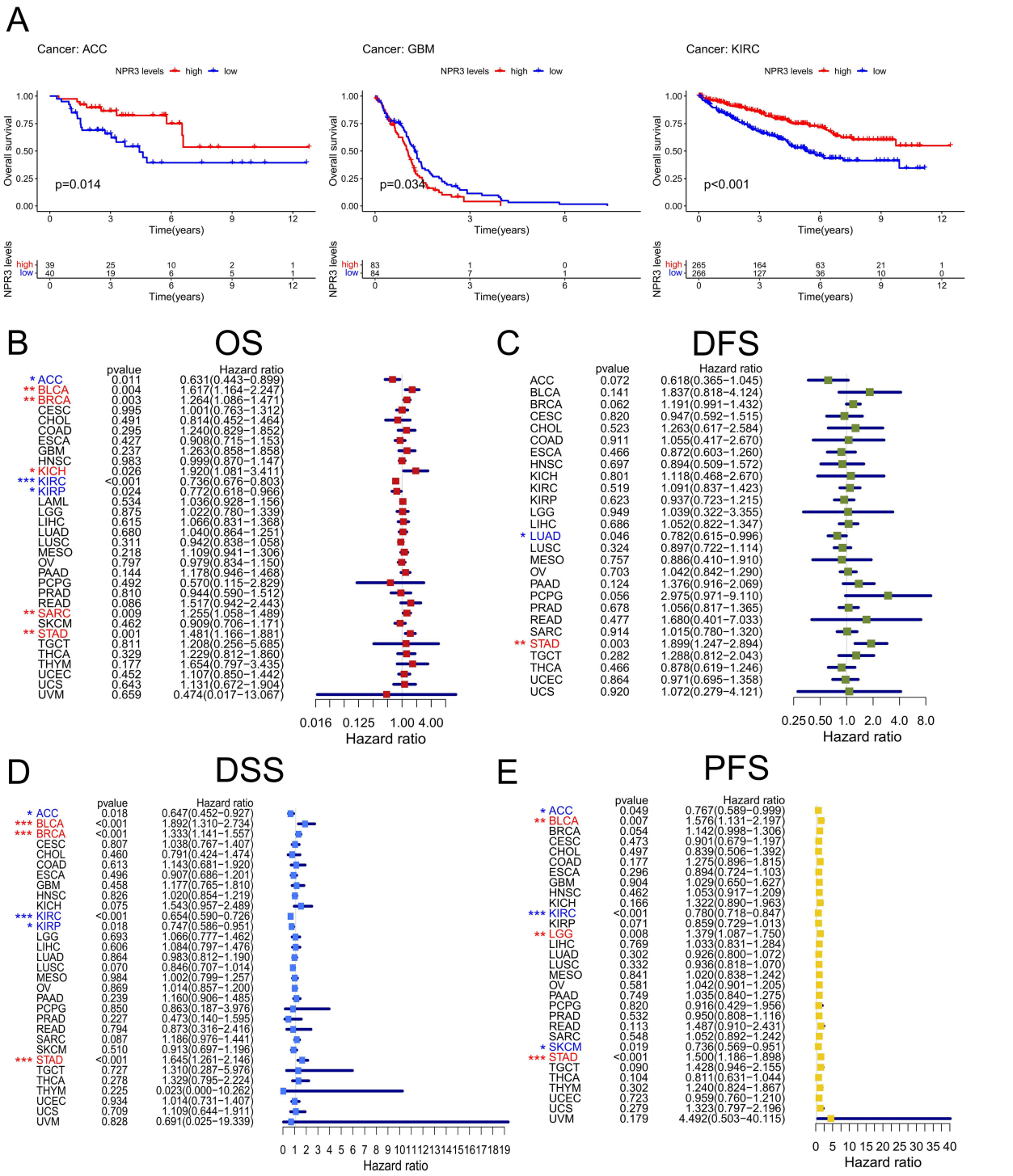

Figure 2 Survival analysis and univariate Cox regression analysis in pan-cancer. (**A**) KM curve in ACC, GBM and KIRC. Lower NPR3 expression was related with better OS in patients of GBM, while higher NPR3 was correlated with better OS in ACC and KIRC. (**B**) Univariate Cox model of OS. NPR3 expression was a risk factor in BLCA (HR = 1.617, 95% CI = 1.164–2.247, $p = 0.004$), BRCA (HR = 1.264, 95% CI = 1.086–1.471, $p = 0.003$), KICH (HR = 1.920, 95% CI = 1.081–3.411, $p < 0.001$), SARC (HR = 1.255, 95% CI = 1.058–1.489, $p = 0.009$) and STAD (HR = 1.481, 95% CI = 1.166–1.881, $p = 0.001$), and it was a protective factor in ACC (HR = 0.631, 95% CI = 0.443–0.899, $p = 0.011$), KIRC (HR = 0.736, 95% CI = 0.676–0.803, $p < 0.001$) and KIRP (HR = 0.772, 95% CI = 0.618–0.966, $p = 0.024$). (**C**) Univariate Cox model of DFS. NPR3 expression was a risk factor in STAD (HR = 1.90, 95% CI = 1.25–2.89, $p = 0.003$), while it was a protective factor in LUAD (HR = 0.78, 95% CI = 0.61–1.00, $p = 0.046$). (**D**) Univariate Cox model in DSS. NPR3 expression was a risk factor in STAD (HR = 1.64, 95% CI = 1.26–2.15, $p < 0.001$), BRCA (HR = 1.33, 95% CI = 1.14–1.56, $p < 0.001$) and BLCA (HR = 1.89, 95% CI = 1.31–2.73, $p < 0.001$), while it was a protective factor in KIRC (HR = 0.65, 95% CI = 0.59–0.73, $p < 0.001$), ACC (HR = 0.65, 95% CI = 0.45–0.93, $p = 0.018$) and KIRP (HR = 0.75, 95% CI = 0.59–0.95, $p = 0.018$). (**E**) Univariate Cox model in PFS. NPR3 expression was a risk factor in STAD (HR = 1.50, 95% CI = 1.19–1.90, $p < 0.001$), BLCA (HR = 1.58, 95% CI = 1.13–2.20, $p = 0.007$) and LGG (HR = 1.38, 95% CI = 1.09–1.75, $p = 0.008$), while it was a protective factor in KIRC (HR = 0.78, 95% CI = 0.72–0.85, $p < 0.001$), SKCM (HR = 0.74, 95% CI = 0.57–0.95, $p = 0.019$) and ACC (HR = 0.77, 95% CI = 0.59–1.00, $p = 0.049$). *$p < 0.05$, **$p < 0.01$, ***$p < 0.001$.

Abbreviations: OS, Overall survival; DFS, Disease-free survival; DSS, Disease-specific survival; PFS, Progression-free survival.

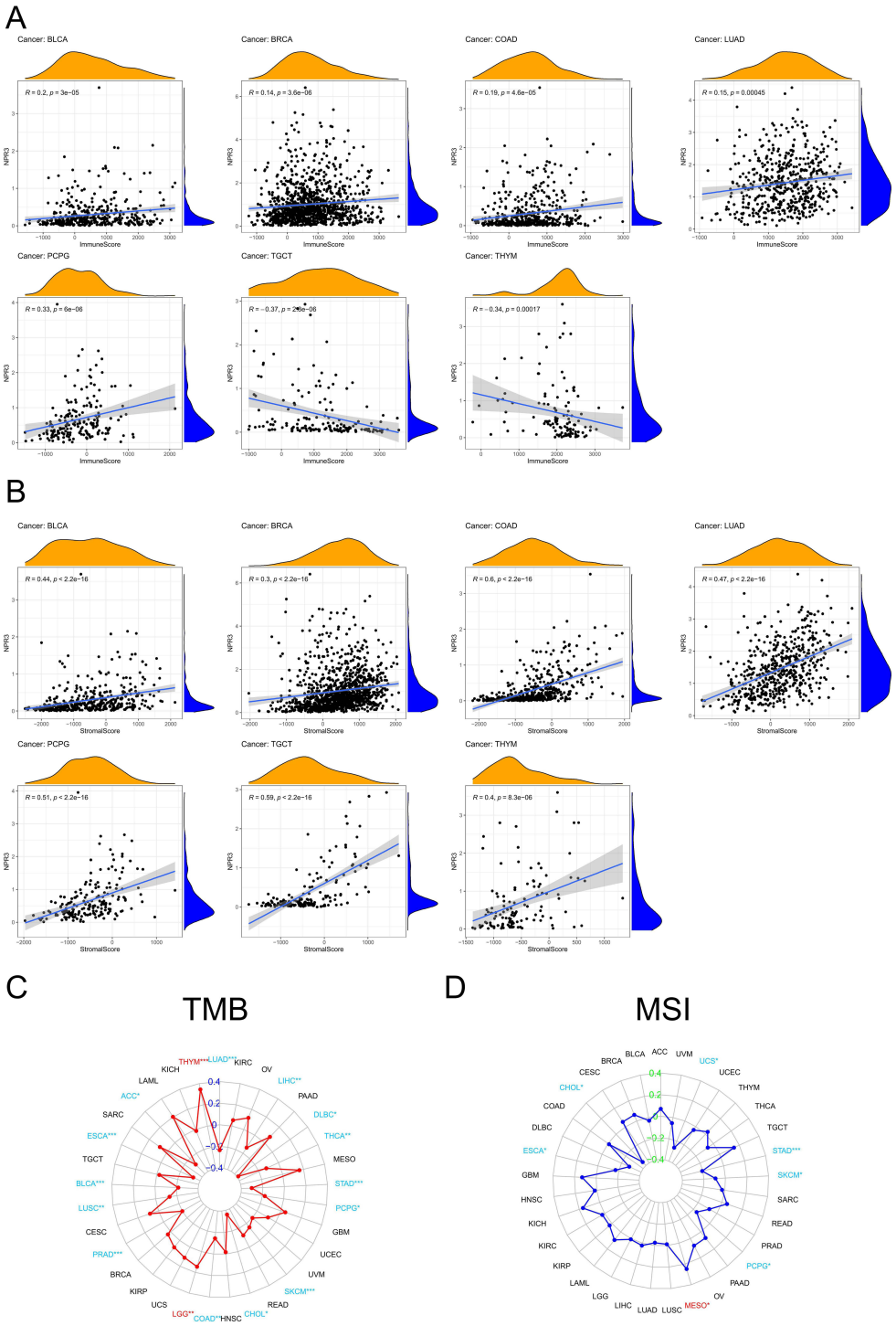

Figure 3 Relationship of NPR3 expression with TME, TMB and MSI in pan-cancer. (**A**) Correlation of NPR3 expression with immune scores. It was positively correlated with immune scores in BLCA (R = 0.2, $p < 0.001$), BRCA (R = 0.14, $p < 0.001$), COAD (R = 0.19, $p < 0.001$), LUAD (R = 0.15, $p < 0.001$) and PCPG (R = 0.33, $p < 0.001$), while it was negatively correlated in TGCT (R = −0.37, $p < 0.001$), and THYM (R = −0.34, $p < 0.001$). (**B**) Correlation of NPR3 expression with stromal scores. It was positively correlated with stromal scores in BLCA (R = 0.44, $p < 0.001$), BRCA (R = 0.3, $p < 0.001$), COAD (R = 0.6, $p < 0.001$), LUAD (R = 0.47, $p < 0.001$), PCPG (R = 0.51, $p < 0.001$), PRAD (R = 0.15, $p < 0.001$), TGCT (R = 0.59, $p < 0.001$) and THYM (R = 0.4, $p < 0.001$). (**C**) Correlation of NPR3 expression with TMB. It was positively correlated with TMB in THYM ($p < 0.001$) and LGG ($p < 0.001$), while it was negatively correlated in LUAD ($p < 0.001$), ACC ($p < 0.05$), ESCA ($p < 0.001$), BLCA ($p < 0.001$), LUSC ($p < 0.01$), PRAD ($p < 0.001$), COAD ($p < 0.01$), CHOL ($p < 0.05$), SKCM ($p < 0.001$), PCPG ($p < 0.05$), STAD ($p < 0.001$), THCA ($p < 0.01$), DLBC ($p < 0.05$) and LIHC ($p < 0.01$). (**D**) Correlation of NPR3 expression with MSI. It was positively correlated with MSI in MESO ($p < 0.05$), while it was negatively related in CHOL ($p < 0.05$), ESCA ($p < 0.05$), PCPG ($p < 0.05$), SKCM ($p < 0.05$), STAD ($p < 0.001$) and UCS ($p < 0.05$). *$p < 0.05$, **$p < 0.01$, ***$p < 0.001$.

Abbreviations: TME, Tumor microenvironment; TMB, Tumor mutation burden; MSI, Microsatellite instability.

https://doi.org/10.2147/JIR.S515347

TME Analysis in Pan-Cancer

A significant association was observed between NPR3 expression and genes related with immunity, including NRP1, TNFSF18, and NFRSF14. Additionally, most immune genes exhibited a negative correlation with NPR3 expression in KIRC, TGCT, THCA, and THYM (Figure 4A).

To further investigate immune infiltration, the ESTIMATE algorithm was employed, and the significant association between NPR3 expression and specific immune cell types was elucidated (Figures 4B and S8).

Further analysis using the TIMER 2.0 database revealed that NPR3 expression, in most cancer types, showed positive correlation with cancer-associated fibroblasts (CAF) and endothelial cells (Figure S9).

Additionally, CTL infiltration and survival analyses were performed using the TIDE database (Table S2). A negative association between NPR3 expression and CTL infiltration was indicated in BRCA (Figure S10A). Survival analysis suggested that lower NPR3 expression correlated with improved survival in UCEC (Figure S10B). Additionally, Cox regression analysis indicated that reduced NPR3 expression was linked to impaired CTL function in UCEC (Figure S10C).

Predicting NPR3-Related Drug Sensitivity in Pan-Cancer

After that, we conducted drug sensitivity prediction for NPR3 depending on CTRP, GDSC, and CellMiner databases (Figure 5A–C). Increased NPR3 expression was associated with reduced sensitivity to most drugs, particularly selumetinib and voreloxin. However, several drugs showed higher sensitivity in higher NPR3 expression, including tamatinib and dasatinib from CTRP, midostaurin and tivozanib from GDSC, and Bisacodyl and Acetalax from CellMiner. This suggests that NPR3 may be involved in specific cancer–drug interactions, and drugs targeting NPR3 could prove valuable in future anti-cancer therapies.

The potential binding interaction between NPR3 and dasatinib was assessed through molecular docking analysis, and the results were visualized in 3D. Dasatinib exhibited the lowest binding affinity of −7.8 kcal/mol when interacting with SER-250, ASP-307, and GLU-288 (Figure 5D). Additional binding sites were identified, showing binding energies of −7.7, −7.7, −7.7, −7.6, −7.4, and −7.4 kcal/mol, respectively (Figure S11).

Functional Enrichment Analysis of NPR3 in Pan-Cancer

Using GSEA, we examined the signaling pathways associated with NPR3 expression. The most frequently enriched KEGG pathways in high-NPR3 expression groups included the “regulation of autophagy”, “cytosolic DNA sensing pathway”, “Toll-like receptor signaling pathway”, and “starch and sucrose metabolism”.

The “regulation of autophagy” pathway was down-regulated in BLCA, but up-regulated in LGG, LUSC, and PAAD. The “cytosolic DNA sensing pathway” showed down-regulation in OV, while it was up-regulated in LUSC and PAAD. The “Toll-like receptor signaling pathway” was down-regulated in BLCA and OV, but up-regulated in LUSC. Finally, the “starch and sucrose metabolism” pathway was up-regulated in ACC, HNSC, and SKCM (Figure S12).

Baseline Information of the Retrospective Cohort with Kidney Neoplasm

After an initial examination of NPR3 across various cancers, we identified several significant findings in kidney neoplasms. This discovery prompted us to conduct a clinical validation of NPR3 in patients with kidney neoplasms.

The inclusion and exclusion criteria are outlined in Figure 6A, while the demographic and clinical characteristics are presented in Table 1 and Figure S13A. Regarding histopathological classification, most patients (88.9%) were diagnosed with KIRC, followed by smaller proportions diagnosed with KIRP (4.9%), KICH (2.2%), and other kidney neoplasms (4.1%). According to Fuhrman nuclear staging, the distribution of patients was as follows: 18.6% of Stage 1, 63.2% of Stage 2, 13.8% of Stage 3, and 4.3% of Stage 4. Notably, a substantial number of patients were diagnosed at intermediate clinical stages, with “Stage II” and “Stage III” (14.7% and 63.8%, respectively) accounting for the majority of cases. In terms of clinical indicators, 74.6% of patients were alive, and the majority (69.5%) of patients experienced no disease progression.

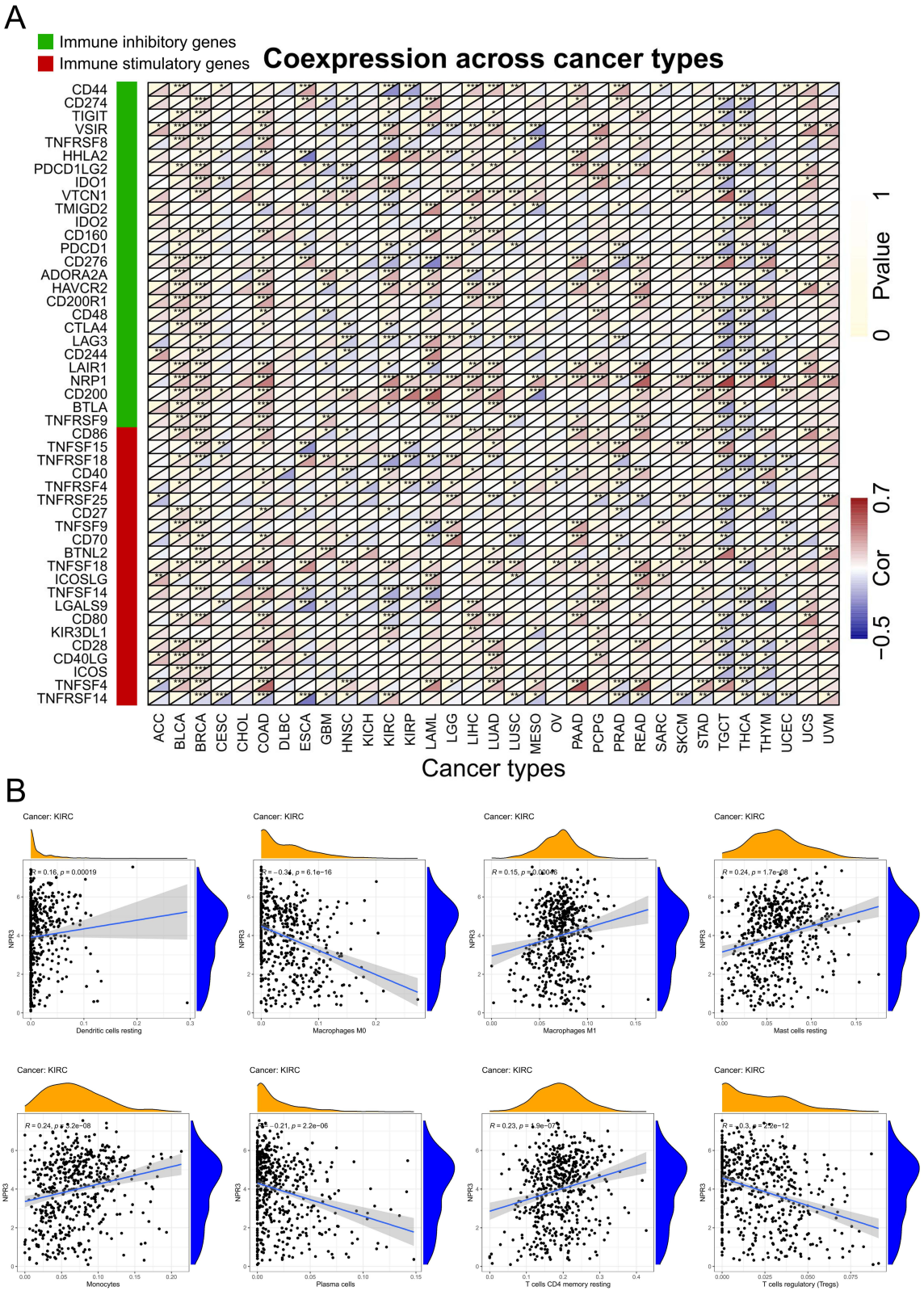

Figure 4 Co-expression of NPR3 immune related genes and immune infiltration analysis in KIRC. (**A**) The relationship between NPR3 expression and immune-related genes. NPR3 expression exhibited a significant correlation with several immune genes expression among pan-cancer, including NRP1, TNFSF18 and NFRSF14. Besides, most of the immune genes were negatively correlated with NPR3 expression in KIRC, TGCT, THCA and THYM. (**B**) In KIRC, NPR3 expression was positively correlated with dendritic cells resting (R = 0.16, $p < 0.001$), macrophages M1 (R = 0.15, $p < 0.001$), mast cells resting (R = 0.24, $p < 0.001$), monocytes (R = 0.24, $p < 0.001$) and T cells CD4 memory resting (R = 0.23, $p < 0.001$), while it was negatively correlated with macrophages M0 (R = −0.34, $p < 0.001$), plasma cells (R = −0.21, $p < 0.001$) and T cells regulatory (R = −0.3, $p < 0.001$).

https://doi.org/10.2147/JIR.S515347

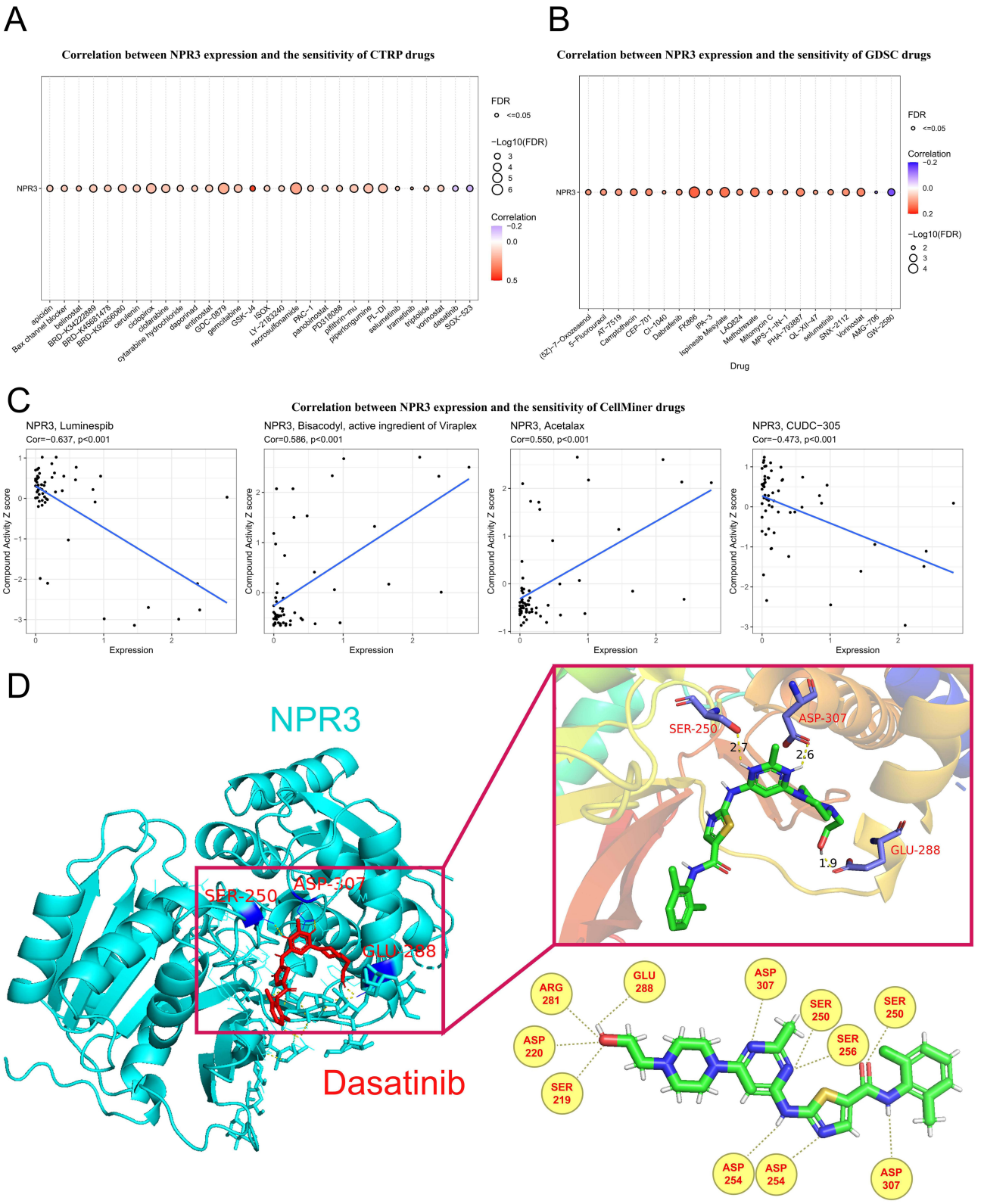

Figure 5 Drug sensitivity prediction for NPR3 in (**A**) CTRP, (**B**) GDSC and (**C**) CellMiner databases. Higher expression of NPR3 was related with lower drug sensitivity of most drugs, especially selumetinib and voreloxin. However, several drugs showed higher sensitivity in higher NPR3 expression, including dasatinib and SGX-523 from CTRP, AMG-706 and GW-2580 from GDSC, and Bisacodyl and Acetalax from CellMiner. (**D**) Molecular docking of NPR3 protein with dasatinib. The possible binding sites were all illustrated.

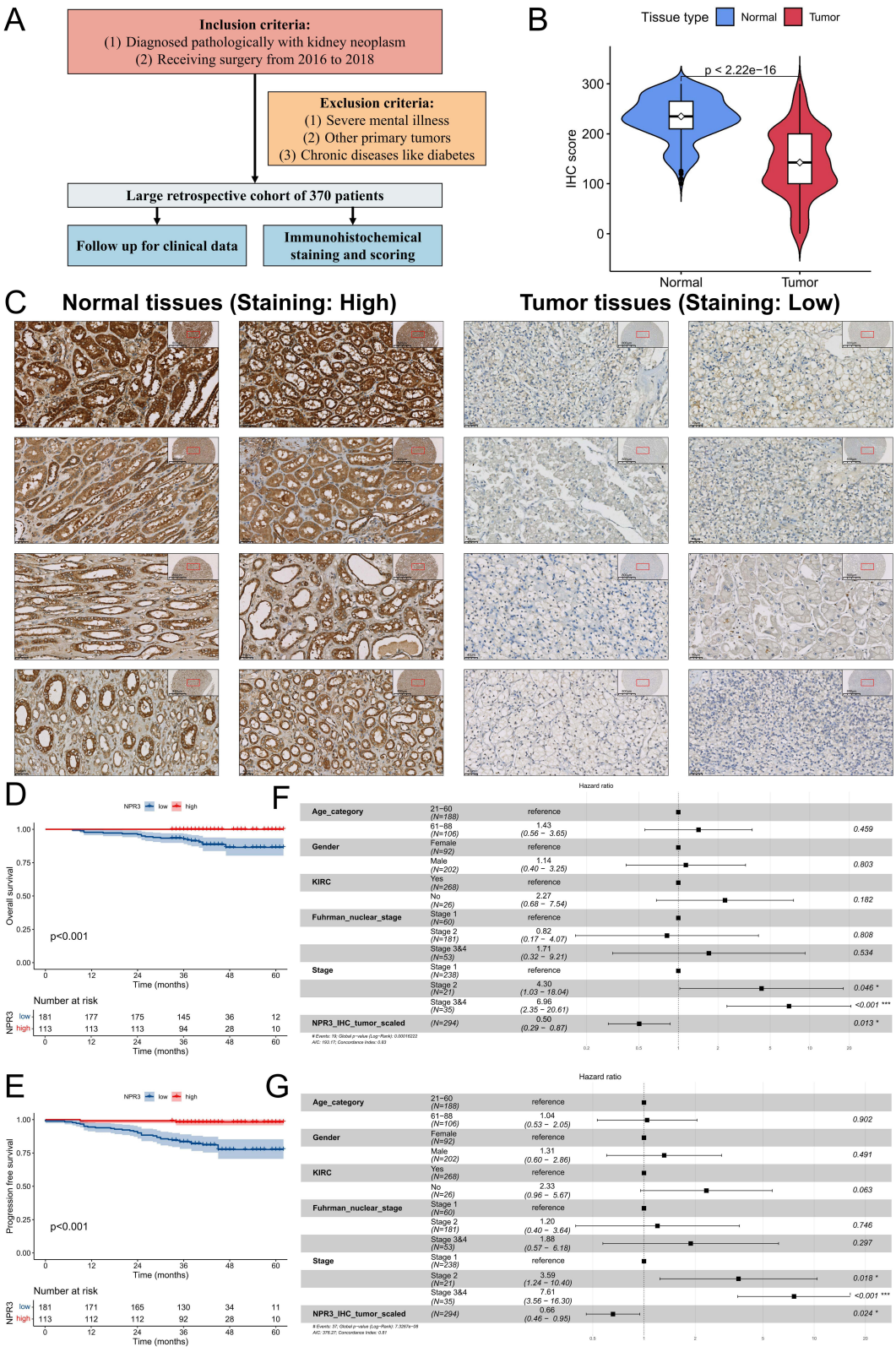

Figure 6 Higher NPR3 expression was associated with better prognosis in kidney neoplasms. (**A**) The inclusion and exclusion criteria of the cohort. (**B**) The IHC scores of normal tissue were significantly higher than those of tumor tissues ($p < 0.001$). (**C**) Several representative IHC pictures of kidney neoplasm tissue and normal ones from the cohort. The K-M survival curve indicated that higher NPR3 expression was correlated with better (**D**) OS and (**E**) PFS in kidney neoplasm ($p < 0.001$). (**F**) Multivariate Cox regression analysis indicated that NPR3 expression, presented by scaled IHC score through Z-score transformation, was an independent protective factor for OS (HR = 0.50, 95% CI = 0.29–0.87, $p = 0.0133$). (**G**) Multivariate Cox regression analysis indicated that NPR3 expression, presented by scaled IHC score through Z-score transformation, was an independent protective factor for PFS (HR = 0.66, 95% CI = 0.46–0.95, $p = 0.0236$).

Abbreviations: IHC, Immunohistochemical; HR, Hazard ratio; OS, Overall survival; PFS, Progression-free survival.

https://doi.org/10.2147/JIR.S515347

Table 1 | Demographic Characteristics of 370 Patients

Variables	Number (%)	Mean ± SD	Median (Range)	P-value
NPR3 tumor		142.49 ± 66.33	140 (0–300)	
NPR3 classification tumor				
Low (IHC score of NPR3 <= 150)	221 (59.73)			
High (IHC score of NPR3 > 150)	148 (40.00)			
Unknown	1 (0.27)			
NPR3 normal		230.83 ± 44.15	235 (100–300)	
NPR3 classification normal				< 0.001***
Low (IHC score of NPR3 <= 150)	25 (6.76)			
High (IHC score of NPR3 > 150)	286 (77.30)			
Unknown	59 (15.94)			
OS censor				
Alive	276 (74.59)			
Dead	23 (6.22)			
Unknown	71 (19.19)			
OS		42.24 ± 9.34	41 (7–62)	
OS classification (months)				
Low (OS <=41)	155 (41.89)			
High (OS > 41)	140 (37.84)			
Unknown	75 (20.27)			
PFS censor				
No	257 (69.46)			
Yes	42 (11.35)			
Unknown	71 (19.19)			
PFS		40.99 ± 10.95	41 (0–62)	
PFS classification (months)				
Low (PFS <=41)	161 (43.51)			
High (PFS > 41)	134 (36.22)			
Unknown	75 (20.27)			
Age (category)				
21-55	186 (50.27)			
56-88	184 (49.73)			
Gender				
Female	114 (30.81)			
Male	256 (69.19)			
KIRC				
No	41 (11.08)			
Yes	329 (88.92)			
Histopathological classification				
KIRC	329 (88.92)			
KIRP	18 (4.86)			
KICH	8 (2.16)			
Others	15 (4.05)			
Fuhrman nuclear stage				< 0.05*
Stage 1	69 (18.65)			
Stage 2	234 (63.24)			
Stage 3	51 (13.78)			
Stage 4	16 (4.32)			

(*Continued*)

Table 1 (Continued).

Variables	Number (%)	Mean ± SD	Median (Range)	P-value
T stage				< 0.05*
T1	282 (76.22)			
T2	29 (7.84)			
T3	53 (14.32)			
T4	3 (0.81)			
Unknown	3 (0.81)			
Detailed T stage				
T1a	178 (48.11)			
T1b	104 (28.11)			
T2a	17 (4.59)			
T2b	12 (3.24)			
T3a	49 (13.24)			
T3b	2 (0.54)			
T3c	2 (0.54)			
T4	3 (0.81)			
Unknown	3 (0.81)			
N stage				
N0	368 (99.46)			
N1	2 (0.54)			
M stage				
M0	370 (100.00)			
Stage				< 0.05*
Stage 1	282 (76.22)			
Stage 2	28 (7.57)			
Stage 3	54 (14.59)			
Stage 4	3 (0.81)			
Unknown	3 (0.81)			
Progression after treatment				
No	258 (69.73)			
Yes	41 (11.08)			
Unknown	71 (19.19)			

Notes: *p < 0.05, ***p < 0.001.
Abbreviations: IHC, Immunohistochemical; OS, overall survival; PFS, progression free survival; KIRC, kidney renal clear cell carcinoma; KICH, kidney chromophobe; KIRP, kidney renal papillary cell carcinoma.

Investigation of NPR3 Expression and Clinical Relevance in Kidney Neoplasms

IHC staining was performed on tumor and normal tissues from 370 patients. NPR3 was significantly down-regulated in kidney neoplasms ($p < 0.001$) with the mean IHC score of 142.49 in tumor tissues and 230.83 in normal ones (Figure 6B). Typical IHC staining images of both tumor tissues and normal ones from the cohort are shown in Figure 6C.

Using the "surv_cutpoint" function, we determined the optimal cut-off values for the IHC score of NPR3 in tumor tissues (150 for both OS and PFS) (Figure S13B and S13C). K-M survival curves showed that higher NPR3 expression (IHC score > 150) in tumor tissues was significantly linked to better OS ($p < 0.001$, Figure 6D) and PFS ($p < 0.001$, Figure 6E), compared to lower NPR3 expression (IHC score ≤ 150). Subsequently, after conducting Z-score transformation to normalize the IHC score of NPR3 for better and deeper data presentation, we used the scaled NPR3 IHC score as a continuous variable for univariate and multivariate Cox regression analysis. Results demonstrated that, NPR3 expression was a significant protective factor in both univariate Cox regression analysis (HR = 0.55, 95% CI = 0.35–0.89, $p = 0.014$, Figure S13D) and multivariate Cox regression analysis (HR = 0.50, 95% CI = 0.29–0.87, $p = 0.013$, Figure 6F) for OS in RCC patients. Additionally, NPR3 expression was also identified as a significant protective factor in both univariate Cox regression analysis (HR = 0.67, 95% CI = 0.47–0.93, $p = 0.018$, Figure S13D) and multivariate Cox

regression analysis (HR = 0.66, 95% CI = 0.46–0.95, $p = 0.024$, Figure 6G) for PFS in RCC patients. Consequently, we concluded that NPR3 expression was an independent protective factor for both OS and PFS in RCC patients, excluding the confounding factors of age, gender, histopathological classification, Fuhrman nuclear stage, and stage.

The deviance residual plot showed that, for both models, the residuals were randomly scattered about zero with no clear pattern (Figure S14A and S14G). The calibration curves showed that the predicted 1-, 2-, 3-, 4-, and 5-year-OS (Figure S14B) and 1-, 2-, 3-, 4-, and 5-year-PFS (Figure S14H) closely matched with the actual outcomes. The ROC curves provided the area under curve (AUC) at 1 year (0.922), 2 years (0.809), 3 years (0.804), 4 years (0.915), and 5 years (0.928) for OS (Figure S14C). For PFS, AUC of the ROC curves at 1 year (0.865), 2 years (0.821), 3 years (0.813), 4 years (0.862), and 5 years (0.856) were also provided (Figure S14I). Risk models were constructed according to both models (Figure S14D and S14J), and K-M survival curve demonstrated that patients with higher risk scores had significantly poorer OS ($p < 0.001$) (Figure S14E and S14K). At last, nomograms were constructed for predicting 1-, 2-, 3-, 4-, and 5-year OS probability and PFS probability for kidney neoplasm patients (Figure S14F and S14L).

External Validation for NPR3 Expression in Kidney Neoplasms

In PDC000464, GSE36895, GSE53757, GSE66272, GSE126964, and GSE167093, the differential expression analysis confirmed that NPR3 expression was significantly downregulated in kidney neoplasms ($p < 0.001$) compared to normal tissues, which aligns with our findings (Figure S15A). In PDC000127, PDC000464, GSE22541, and RCC_2020_Braun_Cohort, K-M survival curves showed that higher NPR3 expression was significantly associated with better survival outcomes ($p < 0.05$) in kidney neoplasm patients, further supporting our results (Figure S15B).

Knockdown of NPR3 in 786-O, 769-P, and A-498 Cells Suppressed Cell Proliferation, Migration, and Invasion

After the cohort validation, we created a stable NPR3 knockdown cell line using shRNA. qPCR and Western blot results confirmed NPR3 expression significantly decreased in the knockdown cells compared to the control group ($p < 0.05$) (Figure 7A). The colony formation assay suggested decreased proliferation ability in NPR3 knockdown cells ($p < 0.001$) (Figure 7B). The CCK-8 assay demonstrated that NPR3 inhibition caused marked reduction in cell proliferation ability after 72 hours ($p < 0.01$) (Figure 7C). The transwell migration and invasion assays demonstrated that NPR3 knockdown cells exhibited a significant reduction in both migratory ($p < 0.05$) and invasive ($p < 0.001$) capabilities (Figure 7D and E). The cell scratch assay showed that NPR3 knockdown cells exhibited significantly weaker migration ability compared to control cells 24 hours post-scratching ($p < 0.05$) (Figure 7F). Interestingly, treatment with dasatinib appeared to enhance NPR3 expression in human renal cancer cells (Figure S16).

Discussion

NPR3, one member of the receptor for natriuretic peptides (NP), is reported to play a wide range of physiological roles, including plant immunity,[74] neural crest and cranial placode formation,[75] apoptosis in cardiomyocytes,[76] and insulin sensitivity,[77] but few studies have elucidated its specific role in pan-cancer. Our study provided differential expression analysis, ceRNA and PPI network construction, clinical relevance analysis, tumor purity analysis, genetic mutation analysis, immune infiltration analysis, and signaling pathway enrichment analysis. Then, a retrospective cohort of kidney neoplasms was investigated, and NPR3 was identified as a potential biomarker for kidney neoplasm development. Clinical relevance analysis was conducted for validation. Besides, cell experiment was conducted that NPR3-knockdown significantly suppressed tumor proliferative and migration activity in renal cancer cells. Our study revealed that NPR3 was a potential biomarker for predicting the efficacy of immunotherapy and guiding cancer therapy.

NPR3 Might Be a Potential Biomarker in Various Cancers

Previous researches have explored that NPR3 is correlated with tumor development and patients' prognosis, and controversial results have been reported. Gu et al reported that, in colorectal cancer cells, up-regulated NPR3 may promote the proliferation as well as inhibiting apoptosis.[9] However, opposition was proposed by Li et al that the

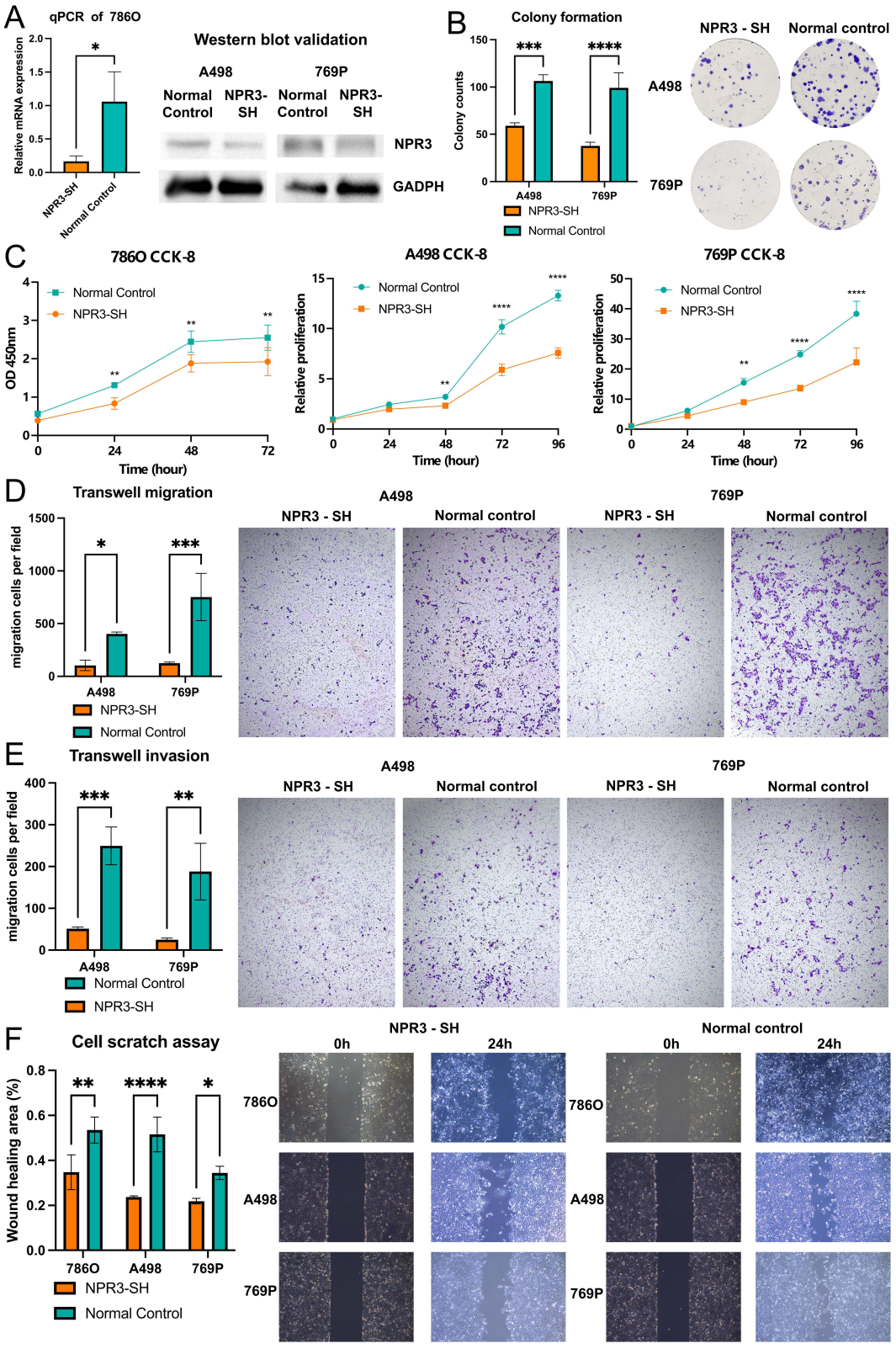

Figure 7 Knockdown of NPR3 in 786-O, 769-P, and A-498 cells suppressed cell proliferation, migration, and invasion. (**A**) The qPCR analysis and Western blot validation showed that NPR3 expression in NPR3-sh cells was significantly lower than that in control cells. (**B**) The colony formation assay suggested decreased proliferation in NPR3-sh cells. (**C**) The CCK-8 assay indicated reduced cell proliferation in NPR3 knockdown cells. (**D**) The transwell migration assay indicated decreased migration in NPR3-sh cells. (**E**) The transwell invasion assay indicated decreased invasion in NPR3-sh cells. (**F**) The cell scratch assay showed suppressed wound healing ability in NPR3-sh cells. *$p < 0.05$, **$p < 0.01$, ***$p < 0.001$.
Abbreviations: qPCR, quantitative real-time polymerase-chain reaction; CCK-8, Cell counting kit-8; NC, Normal control.

https://doi.org/10.2147/JIR.S515347

repression of NPR3 could promote the metastasis of clear cell renal cell carcinoma.[11] Likewise, Qian et al found that NPR3 overexpression inhibited the development and progression of hepatocellular carcinoma cells.[12] Li et al found that NPR3 inhibits tumor cell growth in osteosarcoma.[14] In our pan-cancer analysis, we observed that NPR3 expression was significantly reduced in 14 tumor types when compared to normal tissues. Survival analysis and univariate Cox regression models further revealed that NPR3 expression was significantly related with OS, DSS, DFS, and PFS across various cancer types. Regarding clinical stage, NPR3 showed positive correlation with the clinical stages of COAD and READ, but negatively correlation was observed in KIRC. In our clinical validation, we established a retrospective cohort and observed that NPR3 expression was notably lower in the tumor tissues of kidney neoplasm patients. Moreover, patients exhibiting reduced NPR3 expression demonstrated a marked increase in OS. In renal carcinoma cells, silencing NPR3 led to a substantial reduction in tumor growth and wound-healing capacity. In summary, these findings suggest that NPR3 severs as a prognostic biomarker in cancers, offering clinical implications for patient prognostic prediction.

An Initial Exploration of the Role of NPR3 in Tumor Immunity and Therapy

NPR3 Plays a Role in TME

The TME is composed of a diverse array of cell types, all of which significantly contribute to tumor growth, metastasis, and therapeutic response.[78,79] Immune cells within the TME play crucial roles in either inhibiting or promoting tumor development, depending on the context of the tumorigenic process.[80] NPR3 has been identified as a gene related with immunity in several studies, particularly in breast cancer, where higher NPR3 expression was linked to reduced infiltration of B cells, CD8+ T cells, and dendritic cells,[81,82] as well as lower expression levels of PD-1, PD-L1, and CTLA-4.[83] Despite these findings, the exact role of NPR3 within the TME remains underexplored. In our analysis, we discovered that higher NPR3 expression showed positive correlation with immune scores in BLCA, BRCA, COAD, and LUAD, whereas it showed negative correlation in GBM, HNSC, TGCT, THCA, and THYM. Regarding immune gene co-expression, NPR3 tended to exhibit an immune-suppressive function in pan-cancer, particularly in KIRC, TGCT, THCA, and THYM, where it showed strong associations with macrophages and CD4+ T cells. Additionally, data from the TIMER 2.0 database revealed a consistent positive correlation between NPR3 and CAFs, as well as endothelial cells across various tumor types. CAFs are important in tumor progression by facilitating cancer cell proliferation, enhancing therapy resistance, and promoting immune exclusion.[84,85] They can release cytokines, growth factors, creating extracellular matrix (ECM) structure and reprogramming the tumor microenvironment, leading to resistance to chemotherapy and tumor progression.[86] Besides, endothelial cells are critical components for tumor associated angiogenesis, and they are also one of the main sources of CAF.[87] Moreover, endothelial cells can undergo endothelial-to-mesenchymal transition, which enhances the microenvironment of stromal fibroblasts and reshapes the vessels to support the invasion and metastasis.[88] The correlation between NPR3 expression, CAFs, and endothelial cells might explain the function of NPR3 in pan-cancer. Furthermore, NPR3 may regulate tumor-associated macrophages. NPR3 expression has been shown to block the PI3K/AKT pathway in osteosarcoma cells,[14] which could influence the differentiation of M2 macrophages.[89] This, in turn, may promote angiogenesis, neovascularization, and matrix activation and remodeling—processes that contribute to cancer progression and impact patient outcomes.[90,91] In conclusion, NPR3 expression is correlated with the composition of TME and is worth further investigation.

CTLs, one of the critical immune surveillance cells, are also imperative TME and patient prognosis.[92] A high level of well-functioning CTLs in TME is a positive prognostic predictor, and it can help control tumor progression.[93] However, CTL dysfunction and exclusion are two mechanisms of tumor immune evasion.[43] In our study, the negative correlation between NPR3 and CTL infiltration was found in BRCA. Additionally, in UCEC, tumors with low NPR3 expression exhibited exhausted infiltrating CTLs. To put everything in a nutshell, NPR3 may participate in tumor immunity through its interaction with CTLs.

NPR3 is a Potential Indicator for Immunotherapy

Apart from that, TMB and MSI are two important biomarkers of prognosis in multiple tumors, as well as reliable predictors in immunotherapy.[94,95] Our investigation revealed significant relationships between NPR3 expression and TMB in 16 tumor types and with MSI in 7 tumor types, predominantly exhibiting negative correlations. Based on these findings, we can infer

that NPR3 levels may influence TMB and MSI, potentially affecting the effectiveness of immunotherapy. TMB has become an important predictor of immune checkpoint blockade (ICB) efficacy and serves as a valuable biomarker for identifying patients who are likely to benefit from immunotherapy in certain cancer types. Additionally, a wealth of data supports the use of MSI as a predictor for immunotherapy response and effectiveness. These results highlight the potential advantages of NPR3 expression in guiding ICB therapies.[95–98] What's more, cBioportal analysis and the GSCA database both unveiled the mutation pattern of NPR3. Given that tumors characterized by high levels of somatic mutations resulting from mismatch-repair deficiencies exhibit increased sensitivity to PD-1 targeted therapy, NPR3 may have promising applications in predicting ICB therapeutic response.[99]

Function Analysis Reveals That NPR3 is Correlated with Immunity and Autophagy

Curious about tumorigenesis, we performed GSEA to identify the signaling pathways associated with NPR3 expression. Four pathways emerged as the most strongly associated with NPR3, including "regulation of autophagy", "cytosolic DNA sensing pathway", "Toll-like receptor signaling pathway", and "starch and sucrose metabolism". "Regulation of autophagy" is particularly significant in cancer, as key autophagy-related proteins (such as p53, mTOR, KRAS, etc) and signaling pathways (such as EGFR, PI3K, NFκB, etc) play essential roles in tumor progression.[100] "Cytosolic DNA sensing pathway" is crucial for immune surveillance in tumors, as cancer cells often contain high levels of cytosolic dsDNA, which triggers immune responses.[101] Additionally, "Toll-like receptor signaling pathway" contributes to cancer immunity. Stimulation of Toll-like receptors (TLRs) enhances anti-cancer immune responses, either by activating immune cells or inducing apoptosis.[102,103] Finally, the "starch and sucrose metabolism" pathway has been implicated in the progression of colon cancer. For instance, resistant starch, a type of carbohydrate that bypasses digestion in the small intestine and undergoes fermentation in the large intestine, has been shown to inhibit carcinogenesis in colon epithelial cells.[104] Overall, NPR3 seems to be involved in critical cancer-related processes, particularly immune regulation and autophagy. However, additional studies are required to fully clarify NPR3's function and underlying mechanisms in pan-cancer.

NPR3 Impacts Drug Sensitivity and Potential Therapeutic Strategies in Cancer

We also performed drug sensitivity prediction analysis in order to clarify the therapeutic potential of NPR3. Since higher NPR3 expression was associated with decreased drug sensitivity of most drugs, it implies that NPR3 may involve in mechanisms that lead to greater therapeutic challenges. Few drugs showed higher sensitivity, including tamatinib and dasatinib from CTRP, midostaurin and tivozanib from GDSC, and Bisacodyl and Acetalax from CellMiner. Tamatinib is a selective Syk inhibitor primarily used to treat rheumatoid arthritis, especially in patients who have not responded well to methotrexate treatment.[105,106] Dasatinib, initially discovered as a dual SRC/ABL inhibitor, is a small-molecule tyrosine kinase inhibitor commonly used in managing chronic myelogenous leukemia and Philadelphia chromosome–positive acute lymphoblastic leukemia.[107] Tivozanib, an innovative VEGFR tyrosine kinase inhibitor, is approved as first-line treatment among renal cell carcinoma in adults.[108] Earlier research has demonstrated that tivozanib serves as a viable treatment for patients with recurrent or advancing renal cell carcinoma, even in those who have not responded to prior immunotherapy therapies.[109] Midostaurin, a multi-target kinase inhibitor, is used in the treatment of acute myeloid leukemia.[110] It could inhibit cell growth or inducing apoptosis in various cancer types, blocking angiogenesis, and sensitizing cancer cells to ionizing radiation, thereby justifying its application in cancer therapy.[111] Recent research has also suggested that midostaurin holds potential as an anticancer drug for kidney cancer, as it targets the S100A8 protein.[112] Bisacodyl, a locally acting laxative, operates through a unique dual mechanism that affects gut secretion and motility. It is widely recognized as a standard treatment for constipation.[113] Acetalax (Oxyphenisatin acetate, NSC 59687), a diphenyl oxindole initially used as a laxative, has demonstrated significant cytotoxicity against breast and ovarian cancer cell lines.[114,115] While previous research has not established a direct correlation between NPR3 and the mentioned drugs, these findings offer valuable insights into NPR3's potential pharmaceutical applications in the future. Given that drug sensitivity is positively correlated with NPR3 expression, identifying high NPR3 expression in tumors could guide the use of these drugs for treatment.

The Role of NPR3 in Cancer Requires Further Investigation

In our study, the prognostic outcomes of NPR3 in RCC patients are not consistent with the results from public datasets, this might be attributed to expression-level discrepancies between transcriptomic and proteomic data in RCC tumor, limitation of low-resolution IHC proteomic quantification and 12-point IHC scoring system, limited sample size, and geographical and ethnic differences. Large-sample multicenter clinical study with high-resolution mass spectrum might be needed for further explorations. Moreover, the knockdown of NPR3 in 786-O cells notably inhibited tumor proliferation and migration. This observation, however, contradicts findings from a previous study, which proposed that MRCCAT1 facilitates the progression of KIRC by downregulating NPR3.[11] Specifically, the earlier study showed that MRCCAT1 overexpression increased cell proliferation, migration, and invasion in both 786-O and Caki-1 cells. Additionally, NPR3 mRNA expression was found to be significantly higher in MRCCAT1 knockdown cells and lower in MRCCAT1-overexpressing cells, leading to the conclusion that MRCCAT1 promotes KIRC progression through the suppression of NPR3.[11] The observed discrepancy may stem from differences in experimental strategies. While our study directly knocked down NPR3, reducing its expression, the prior study focused on MRCCAT1 knockdown, which indirectly affected NPR3 expression. These two approaches likely yield distinct biological outcomes. MRCCAT1 might regulate NPR3 via complex transcriptional or epigenetic mechanisms, whereas direct NPR3 knockdown could bypass these regulatory pathways and influence other downstream signaling networks. This suggests that the interaction between MRCCAT1 and NPR3 may not be strictly negative but rather influenced by additional pathways that warrant further exploration. Additionally, NPR3's function appears to be context-dependent, varying across different biological environments. For instance, some studies have implicated NPR3 in promoting tumor development, as observed in colorectal cancer,[9,10] while others have reported tumor-suppressive effects in hepatocellular carcinoma.[12] This duality suggests that NPR3 might exert diverse roles depending on the specific cellular conditions, potentially explaining the discrepancy between results.

Moreover, within the constructed PPI network, NPR3 could bind with atrial natriuretic peptides, including NPPA, NPPB, and NPPC, functioning as a clearance receptor that regulates their local concentrations and biological effects.[116] Moreover, several genes encoding these interacting proteins have been confirmed as oncogenes or tumor suppressors. For instance, knockdown of NPPA enhances the proliferation, migration, and invasion of breast cancer cells.[117] Downregulation of GUCA2B may play a significant role in colorectal tumorigenesis.[118] Further research is needed to explore how these proteins work collectively with NPR3 to exhibit specific functions in tumors.

In conclusion, the precise role of NPR3 in cancer remains ambiguous. Comprehensive research is required to elucidate its mechanisms in different cancers and establish its potential as a therapeutic target.

Limitations

However, some limitations still existed in our study. The small sample size for IHC validation, which limits the generalizability of our findings, and the fact that the clinical retrospective cohort of kidney neoplasm was conducted in China with Chinese patients, may contribute to potential biases. Although the database utilized in our study covered data from Americans, Asians, and Europeans, this could introduce some deviance due to ethnic and geographic differences. Further functional validation, such as in vivo models, is also needed to fully elucidate the biological roles and therapeutic implications of NPR3 in cancer.

Conclusion

In this study, we explored the role of NPR3 in pan-cancer contexts and examined its potential role in the progression of kidney neoplasms using a large retrospective cohort. Our findings suggest that NPR3 may play a significant role in shaping the TME and could serve as an indicator for immunotherapy efficacy. Additionally, NPR3 appears to be correlated with immune functions, autophagy, and drug sensitivity. In renal cancer cells, NPR3 knockdown significantly suppressed tumor proliferation, migration, and invasion activity. While these results highlight NPR3's potential as a biomarker for predicting immunotherapy responses and guiding individualized cancer therapy, further research, including in vivo validation and mechanistic studies, is necessary to fully understand its role in cancer progression and its clinical applicability.

Data Sharing Statement

All data generated and/or analyzed during this study are included in this published article and the supplementary files.

Ethics Approval and Consent to Participate

This study was conducted in accordance with the ethical principles outlined in the Declaration of Helsinki, as revised by the World Medical Association. Written informed consent to participate was obtained from all of the participants in the study. The study was approved by the Ethics Committee of Xinhua Hospital Affiliated to Shanghai Jiao Tong University School of Medicine (XHEC-C-2021-145-1). All authors confirmed that all methods were carried out in accordance with relevant guidelines and regulations.

Acknowledgments

We thank all databases accessed in this study, including the TCGA database for allowing us to use their data.

Author Contributions

All authors made a significant contribution to the work reported, whether that is in the conception, study design, execution, acquisition of data, analysis and interpretation, or in all these areas; took part in drafting, revising or critically reviewing the article; gave final approval of the version to be published; have agreed on the journal to which the article has been submitted; and agree to be accountable for all aspects of the work.

Funding

This work was sponsored by the National Natural Science Foundation of China (No. 82072806); Shanghai Rising-Star Program (23QC1401400); Shanghai Rising-Star Program (Sailing Special Program) (23YF1458400). The funders had no role in study design, data collection and analysis, decision to publish, or preparation of the manuscript.

Disclosure

The authors declare that there are no conflicts of interest.

References

1. Siegel RL, Giaquinto AN, Jemal A. Cancer statistics, 2024. *Ca A Cancer J Clinicians*. 2024;74(1):12–49. doi:10.3322/caac.21820
2. Romero P, Banchereau J, Bhardwaj N, et al. The human vaccines project: a roadmap for cancer vaccine development. *Sci Transl Med*. 2016;8 (334):334ps9. doi:10.1126/scitranslmed.aaf0685
3. Pardoll DM. The blockade of immune checkpoints in cancer immunotherapy. *Nat Rev Cancer*. 2012;12(4):252–264. doi:10.1038/nrc3239
4. Li Q, Ding ZY. The ways of isolating neoantigen-specific T cells. *Front Oncol*. 2020;10:1347. doi:10.3389/fonc.2020.01347
5. Khemlina G, Ikeda S, Kurzrock R. The biology of Hepatocellular carcinoma: implications for genomic and immune therapies. *Mol Cancer*. 2017;16(1):149. doi:10.1186/s12943-017-0712-x
6. Mishra V, Singh A, Chen X, et al. Application of liquid biopsy as multi-functional biomarkers in head and neck cancer. *Br J Cancer*. 2022;126 (3):361–370. doi:10.1038/s41416-021-01626-0
7. Potter LR, Yoder AR, Flora DR, Antos LK, Dickey DM. Natriuretic peptides: their structures, receptors, physiologic functions and therapeutic applications. *Handb Exp Pharmacol*. 2009;2009(191):341–366.
8. Rubattu S, Sciarretta S, Morriello A, et al. NPR-C: a component of the natriuretic peptide family with implications in human diseases. *J Mol Med*. 2010;88(9):889–897. doi:10.1007/s00109-010-0641-2
9. Gu L, Lu L, Zhou D, et al. Long noncoding RNA BCYRN1 promotes the proliferation of colorectal cancer cells via up-regulating NPR3 expression. *Cell Physiol Biochem*. 2018;48(6):2337–2349. doi:10.1159/000492649
10. Martinez-Romero J, Bueno-Fortes S, Martín-Merino M, et al. Survival marker genes of colorectal cancer derived from consistent transcriptomic profiling. *BMC Genomics*. 2018;19(8):45–60. doi:10.1186/s12864-018-5193-9
11. Li J-K, Chen C, Liu J-Y, et al. Long noncoding RNA MRCCAT1 promotes metastasis of clear cell renal cell carcinoma via inhibiting NPR3 and activating p38-MAPK signaling. *Mol Cancer*. 2017;16(1):1–14. doi:10.1186/s12943-017-0681-0
12. Qian G, Jin X, Zhang L. LncRNA FENDRR upregulation promotes hepatic carcinoma cells apoptosis by targeting miR-362-5p via NPR3 and p38-MAPK pathway. *Cancer Biother Radiopharm*. 2020;35(9):629–639. doi:10.1089/cbr.2019.3468
13. Yang Z, Chen Y, Fu Y, et al. Meta-analysis of differentially expressed genes in osteosarcoma based on gene expression data. *BMC Med Genet*. 2014;15(1):1–8. doi:10.1186/1471-2350-15-80
14. Li S, Guo R, Peng Z, et al. NPR3, transcriptionally regulated by POU2F1, inhibits osteosarcoma cell growth through blocking the PI3K/AKT pathway. *Cell Signalling*. 2021;86:110074. doi:10.1016/j.cellsig.2021.110074

15. Liu Y, Dong K, Yao Y, et al. Construction and validation of renal cell carcinoma tumor cell differentiation-related prognostic classification (RCC-TCDC): an integrated bioinformatic analysis and clinical study. *Ann Med*. 2025;57(1):2490830. doi:10.1080/07853890.2025.2490830
16. Lelièvre V, Pineau N, Hu Z, et al. Proliferative actions of natriuretic peptides on neuroblastoma cells. Involvement of guanylyl cyclase and non-guanylyl cyclase pathways. *J Biol Chem*. 2001;276(47):43668–43676. doi:10.1074/jbc.M107341200
17. Prins BA, Weber MJ, Hu R-M, et al. Atrial natriuretic peptide inhibits mitogen-activated protein kinase through the clearance receptor. Potential role in the inhibition of astrocyte proliferation. *J Biol Chem*. 1996;271(24):14156–14162. doi:10.1074/jbc.271.24.14156
18. Rose TL, Kim WY. Renal cell carcinoma: a review. *JAMA*. 2024;332(12):1001–1010. doi:10.1001/jama.2024.12848
19. Bi K, He MX, Bakouny Z, et al. Tumor and immune reprogramming during immunotherapy in advanced renal cell carcinoma. *Cancer Cell*. 2021;39(5):649–661.e5. doi:10.1016/j.ccell.2021.02.015
20. Díaz-Montero CM, Rini BI, Finke JH. The immunology of renal cell carcinoma. *Nat Rev Nephrol*. 2020;16(12):721–735. doi:10.1038/s41581-020-0316-3
21. Li JK, Chen C, Liu J-Y, et al. Long noncoding RNA MRCCAT1 promotes metastasis of clear cell renal cell carcinoma via inhibiting NPR3 and activating p38-MAPK signaling. *Mol Cancer*. 2017;16(1):111.
22. Weinstein JN, Collisson EA, Mills GB, et al. The cancer genome atlas pan-cancer analysis project. *Nat Genet*. 2013;45(10):1113–1120. doi:10.1038/ng.2764
23. Uhlén M, Fagerberg L, Hallström BM, et al. Proteomics. Tissue-based map of the human proteome. *Science*. 2015;347(6220):1260419. doi:10.1126/science.1260419
24. Clark DJ, Dhanasekaran SM, Petralia F, et al. Integrated proteogenomic characterization of clear cell renal cell carcinoma. *Cell*. 2019;179(4):964–983.e31. doi:10.1016/j.cell.2019.10.007
25. Li GX, Chen L, Hsiao Y, et al. Comprehensive proteogenomic characterization of rare kidney tumors. *Cell Rep Med*. 2024;5(5):101547. doi:10.1016/j.xcrm.2024.101547
26. Wuttig D, Zastrow S, Füssel S, et al. CD31, EDNRB and TSPAN7 are promising prognostic markers in clear-cell renal cell carcinoma revealed by genome-wide expression analyses of primary tumors and metastases. *Int J Cancer*. 2012;131(5):E693–704. doi:10.1002/ijc.27419
27. Peña-Llopis S, Vega-rubín-de-celis S, Liao A, et al. BAP1 loss defines a new class of renal cell carcinoma. *Nat Genet*. 2012;44(7):751–759. doi:10.1038/ng.2323
28. Von Roemeling CA, Radisky DC, Marlow LA, et al. Neuronal pentraxin 2 supports clear cell renal cell carcinoma by activating the AMPA-selective glutamate receptor-4. *Cancer Res*. 2014;74(17):4796–4810. doi:10.1158/0008-5472.CAN-14-0210
29. Wotschofsky Z, Gummlich L, Liep J, et al. Integrated microRNA and mRNA signature associated with the transition from the locally confined to the metastasized clear cell renal cell carcinoma exemplified by miR-146-5p. *PLoS One*. 2016;11(2):e0148746. doi:10.1371/journal.pone.0148746
30. Zhao Q, Xue J, Hong B, et al. Transcriptomic characterization and innovative molecular classification of clear cell renal cell carcinoma in the Chinese population. *Cancer Cell Int*. 2020;20(1):461. doi:10.1186/s12935-020-01552-w
31. Laskar RS, Li P, Ecsedi S, et al. Sexual dimorphism in cancer: insights from transcriptional signatures in kidney tissue and renal cell carcinoma. *Hum Mol Genet*. 2021;30(5):343–355. doi:10.1093/hmg/ddab031
32. Braun DA, Hou Y, Bakouny Z, et al. Interplay of somatic alterations and immune infiltration modulates response to PD-1 blockade in advanced clear cell renal cell carcinoma. *Nat Med*. 2020;26(6):909–918. doi:10.1038/s41591-020-0839-y
33. Chen Y, Wang X. miRDB: an online database for prediction of functional microRNA targets. *Nucleic Acids Res*. 2020;48(D1):D127–d131. doi:10.1093/nar/gkz757
34. Jeggari A, Marks DS, Larsson E. miRcode: a map of putative microRNA target sites in the long non-coding transcriptome. *Bioinformatics*. 2012;28(15):2062–2063. doi:10.1093/bioinformatics/bts344
35. Sticht C, De La Torre C, Parveen A, et al. miRWalk: an online resource for prediction of microRNA binding sites. *PLoS One*. 2018;13(10):e0206239. doi:10.1371/journal.pone.0206239
36. Tastsoglou S, Alexiou A, Karagkouni D, et al. DIANA-microT 2023: including predicted targets of virally encoded miRNAs. *Nucleic Acids Res*. 2023;51(W1):W148–w153. doi:10.1093/nar/gkad283
37. Li J-H, Liu S, Zhou H, et al. starBase v2.0: decoding miRNA-ceRNA, miRNA-ncRNA and protein–RNA interaction networks from large-scale CLIP-Seq data. *Nucleic Acids Res*. 2013;42(D1):D92–D97. doi:10.1093/nar/gkt1248
38. Szklarczyk D, Kirsch R, Koutrouli M, et al. The STRING database in 2023: protein-protein association networks and functional enrichment analyses for any sequenced genome of interest. *Nucleic Acids Res*. 2023;51(D1):D638–d646. doi:10.1093/nar/gkac1000
39. Bonneville R, Krook MA, Kautto EA, et al. Landscape of microsatellite instability across 39 cancer types. *JCO Precis Oncol*. 2017;2017:1.
40. Cerami E, Gao J, Dogrusoz U, et al. The cBio cancer genomics portal: an open platform for exploring multidimensional cancer genomics data. *Cancer Discov*. 2012;2(5):401–404. doi:10.1158/2159-8290.CD-12-0095
41. Liu CJ, Hu FF, Xie GY, et al. GSCA: an integrated platform for gene set cancer analysis at genomic, pharmacogenomic and immunogenomic levels. *Brief Bioinform*. 2023;24(1):bbac558.
42. Li T, Fu J, Zeng Z, et al. TIMER2.0 for analysis of tumor-infiltrating immune cells. *Nucleic Acids Res*. 2020;48(W1):W509–w514. doi:10.1093/nar/gkaa407
43. Jiang P, Gu S, Pan D, et al. Signatures of T cell dysfunction and exclusion predict cancer immunotherapy response. *Nat Med*. 2018;24(10):1550–1558. doi:10.1038/s41591-018-0136-1
44. Rees MG, Seashore-Ludlow B, Cheah JH, et al. Correlating chemical sensitivity and basal gene expression reveals mechanism of action. *Nat Chem Biol*. 2016;12(2):109–116. doi:10.1038/nchembio.1986
45. Basu A, Bodycombe N, Cheah J, et al. An interactive resource to identify cancer genetic and lineage dependencies targeted by small molecules. *Cell*. 2013;154(5):1151–1161. doi:10.1016/j.cell.2013.08.003
46. Seashore-Ludlow B, Rees MG, Cheah JH, et al. Harnessing connectivity in a large-scale small-molecule sensitivity dataset. *Cancer Discov*. 2015;5(11):1210–1223. doi:10.1158/2159-8290.CD-15-0235
47. Garnett MJ, Edelman EJ, Heidorn SJ, et al. Systematic identification of genomic markers of drug sensitivity in cancer cells. *Nature*. 2012;483(7391):570–575. doi:10.1038/nature11005

48. Iorio F, Knijnenburg TA, Vis DJ, et al. A landscape of pharmacogenomic interactions in cancer. *Cell*. 2016;166(3):740–754. doi:10.1016/j.cell.2016.06.017
49. Yang W, Soares J, Greninger P, et al. Genomics of drug sensitivity in cancer (GDSC): a resource for therapeutic biomarker discovery in cancer cells. *Nucleic Acids Res*. 2012;41(D1):D955–D961. doi:10.1093/nar/gks1111
50. Shankavaram UT, Varma S, Kane D, et al. CellMiner: a relational database and query tool for the NCI-60 cancer cell lines. *BMC Genomics*. 2009;10(1):277. doi:10.1186/1471-2164-10-277
51. Reinhold WC, Sunshine M, Liu H, et al. CellMiner: a web-based suite of genomic and pharmacologic tools to explore transcript and drug patterns in the NCI-60 cell line set. *Cancer Res*. 2012;72(14):3499–3511. doi:10.1158/0008-5472.CAN-12-1370
52. Kanehisa M, Goto S. KEGG: Kyoto Encyclopedia of Genes and Genomes. *Nucleic Acids Res*. 2000;28(1):27–30. doi:10.1093/nar/28.1.27
53. Andersen PK, Gill RD. Cox's regression model for counting processes: a large sample study. *Ann Stat*. 1982;10(4):1100–1120. doi:10.1214/aos/1176345976
54. Parker JS, Mullins M, Cheang MCU, et al. Supervised risk predictor of breast cancer based on intrinsic subtypes. *J Clin Oncol*. 2009;27(8):1160–1167. doi:10.1200/JCO.2008.18.1370
55. Yoshihara K, Shahmoradgoli M, Martínez E, et al. Inferring tumour purity and stromal and immune cell admixture from expression data. *Nat Commun*. 2013;4(1):2612. doi:10.1038/ncomms3612
56. Newman AM, Liu CL, Green MR, et al. Robust enumeration of cell subsets from tissue expression profiles. *Nat Methods*. 2015;12(5):453–457. doi:10.1038/nmeth.3337
57. Mayakonda A, Lin D-C, Assenov Y, et al. Maftools: efficient and comprehensive analysis of somatic variants in cancer. *Genome Res*. 2018;28(11):1747–1756. doi:10.1101/gr.239244.118
58. The ICGC/TCGA Pan-Cancer Analysis of Whole Genomes Consortium. Pan-cancer analysis of whole genomes. *Nature*. 2020;578(7793):82–93. doi:10.1038/s41586-020-1969-6
59. Zehir A, Benayed R, Shah RH, et al. Mutational landscape of metastatic cancer revealed from prospective clinical sequencing of 10,000 patients. *Nat Med*. 2017;23(6):703–713. doi:10.1038/nm.4333
60. Robinson DR, Wu Y-M, Lonigro RJ, et al. Integrative clinical genomics of metastatic cancer. *Nature*. 2017;548(7667):297–303. doi:10.1038/nature23306
61. Miao D, Margolis CA, Vokes NI, et al. Genomic correlates of response to immune checkpoint blockade in microsatellite-stable solid tumors. *Nat Genet*. 2018;50(9):1271–1281. doi:10.1038/s41588-018-0200-2
62. Hyman DM, Piha-Paul SA, Won H, et al. HER kinase inhibition in patients with HER2- and HER3-mutant cancers. *Nature*. 2018;554(7691):189–194. doi:10.1038/nature25475
63. Samstein RM, Lee C-H, Shoushtari AN, et al. Tumor mutational load predicts survival after immunotherapy across multiple cancer types. *Nat Genet*. 2019;51(2):202–206. doi:10.1038/s41588-018-0312-8
64. Rosen EY, Goldman DA, Hechtman JF, et al. TRK fusions are enriched in cancers with uncommon histologies and the absence of canonical driver mutations. *Clin Cancer Res*. 2020;26(7):1624–1632. doi:10.1158/1078-0432.CCR-19-3165
65. Bolton KL, Ptashkin RN, Gao T, et al. Cancer therapy shapes the fitness landscape of clonal hematopoiesis. *Nat Genet*. 2020;52(11):1219–1226. doi:10.1038/s41588-020-00710-0
66. Wu L, Yao H, Chen H, et al. Landscape of somatic alterations in large-scale solid tumors from an Asian population. *Nat Commun*. 2022;13(1):4264. doi:10.1038/s41467-022-31780-9
67. Nguyen B, Fong C, Luthra A, et al. Genomic characterization of metastatic patterns from prospective clinical sequencing of 25,000 patients. *Cell*. 2022;185(3):563–575.e11. doi:10.1016/j.cell.2022.01.003
68. Barrett T, Wilhite SE, Ledoux P, et al. NCBI GEO: archive for functional genomics data sets--update. *Nucleic Acids Res*. 2013;41(Database issue):D991–5. doi:10.1093/nar/gks1193
69. Curtis C, Shah SP, Chin S-F, et al. The genomic and transcriptomic architecture of 2000 breast tumours reveals novel subgroups. *Nature*. 2012;486(7403):346–352. doi:10.1038/nature10983
70. Morris GM, Huey R, Lindstrom W, et al. AutoDock4 and AutoDockTools4: Automated docking with selective receptor flexibility. *J Comput Chem*. 2009;30(16):2785–2791. doi:10.1002/jcc.21256
71. Trott O, Olson AJ. AutoDock Vina: improving the speed and accuracy of docking with a new scoring function, efficient optimization, and multithreading. *J Comput Chem*. 2010;31(2):455–461. doi:10.1002/jcc.21334
72. Yu G, Wang L-G, Han Y, et al. clusterProfiler: an R package for comparing biological themes among gene clusters. *Omics*. 2012;16(5):284–287. doi:10.1089/omi.2011.0118
73. Wen Z, Luo D, Wang S, et al. Deep Learning-Based H-Score Quantification of Immunohistochemistry-Stained Images. *Mod Pathol*. 2024;37(2):100398. doi:10.1016/j.modpat.2023.100398
74. Ding Y, Sun T, Ao K, et al. Opposite roles of salicylic acid receptors NPR1 and NPR3/NPR4 in transcriptional regulation of plant immunity. *Cell*. 2018;173(6):1454–1467.e15. doi:10.1016/j.cell.2018.03.044
75. Devotta A, Juraver-Geslin H, Griffin C, Saint-Jeannet JP. Npr3 regulates neural crest and cranial placode progenitors formation through its dual function as clearance and signaling receptor. *Elife*. 2023;12:e84036.
76. Lin D, Chai Y, Izadpanah R, et al. NPR3 protects cardiomyocytes from apoptosis through inhibition of cytosolic BRCA1 and TNF-α. *Cell Cycle*. 2016;15(18):2414–2419. doi:10.1080/15384101.2016.1148843
77. Roos J, Dahlhaus M, Funcke J-B, et al. miR-146a regulates insulin sensitivity via NPR3. *Cell Mol Life Sci*. 2021;78(6):2987–3003. doi:10.1007/s00018-020-03699-1
78. Bilotta MT, Antignani A, Fitzgerald DJ. Managing the TME to improve the efficacy of cancer therapy. *Front Immunol*. 2022;13:954992. doi:10.3389/fimmu.2022.954992
79. De Visser KE, Joyce JA. The evolving tumor microenvironment: from cancer initiation to metastatic outgrowth. *Cancer Cell*. 2023;41(3):374–403. doi:10.1016/j.ccell.2023.02.016
80. Lei X, Lei Y, Li J-K, et al. Immune cells within the tumor microenvironment: Biological functions and roles in cancer immunotherapy. *Cancer Lett*. 2020;470:126–133. doi:10.1016/j.canlet.2019.11.009

81. Fu J, Sun H, Xu F, et al. RUNX regulated immune-associated genes predicts prognosis in breast cancer. *Front Genet*. 2022;13:960489. doi:10.3389/fgene.2022.960489
82. Yao Y, Kong X, Liu R, et al. Development of a novel immune-related gene prognostic index for breast cancer. *Front Immunol*. 2022;13:845093. doi:10.3389/fimmu.2022.845093
83. Lv W, He X, Wang Y, et al. A novel immune score model predicting the prognosis and immunotherapy response of breast cancer. *Sci Rep*. 2023;13(1):6403. doi:10.1038/s41598-023-31153-2
84. Chen X, Song E. Turning foes to friends: targeting cancer-associated fibroblasts. *Nat Rev Drug Discov*. 2019;18(2):99–115. doi:10.1038/s41573-018-0004-1
85. Biffi G, Tuveson DA. Diversity and biology of cancer-associated fibroblasts. *Physiol Rev*. 2021;101(1):147–176. doi:10.1152/physrev.00048.2019
86. Kalluri R. The biology and function of fibroblasts in cancer. *Nat Rev Cancer*. 2016;16(9):582–598.
87. Sobierajska K, Ciszewski WM, Sacewicz-Hofman I, Niewiarowska J. Endothelial cells in the tumor microenvironment. *Adv Exp Med Biol*. 2020;1234:71–86.
88. Clere N, Renault S, Corre I. Endothelial-to-mesenchymal transition in cancer. *Front Cell Dev Biol*. 2020;8:747. doi:10.3389/fcell.2020.00747
89. Wu H, Ma T, He M, et al. Cucurbitacin B modulates M2 macrophage differentiation and attenuates osteosarcoma progression via PI3K / AKT pathway. *Phytother Res*. 2024;38(5):2215–2233. doi:10.1002/ptr.8146
90. Afik R, Zigmond E, Vugman M, et al. Tumor macrophages are pivotal constructors of tumor collagenous matrix. *J Exp Med*. 2016;213(11):2315–2331. doi:10.1084/jem.20151193
91. Ruffell B, Coussens LM. Macrophages and therapeutic resistance in cancer. *Cancer Cell*. 2015;27(4):462–472. doi:10.1016/j.ccell.2015.02.015
92. Church SE, Galon J. Regulation of CTL infiltration within the tumor microenvironment. *Adv Exp Med Biol*. 2017;1036:33–49.
93. Mami-Chouaib F, Blanc C, Corgnac S, et al. Resident memory T cells, critical components in tumor immunology. *J Immunother Cancer*. 2018;6(1):87.
94. van Velzen MJM, Derks S, van Grieken NCT, et al. MSI as a predictive factor for treatment outcome of gastroesophageal adenocarcinoma. *Cancer Treat Rev*. 2020;86:102024. doi:10.1016/j.ctrv.2020.102024
95. Chan TA, Yarchoan M, Jaffee E, et al. Development of tumor mutation burden as an immunotherapy biomarker: utility for the oncology clinic. *Ann Oncol*. 2019;30(1):44–56.
96. Gryfe R, Kim H, Hsieh ETK, et al. Tumor microsatellite instability and clinical outcome in young patients with colorectal cancer. *N Engl J Med*. 2000;342(2):69–77. doi:10.1056/NEJM200001133420201
97. Lee DW, Han S-W, Bae JM, et al. Tumor mutation burden and prognosis in patients with colorectal cancer treated with adjuvant fluoropyrimidine and oxaliplatin. *Clin Cancer Res*. 2019;25(20):6141–6147. doi:10.1158/1078-0432.CCR-19-1105
98. Li K, Luo H, Huang L, Luo H, Zhu X, et al. Microsatellite instability: a review of what the oncologist should know. *Cancer Cell Int*. 2020;20:16.
99. Zhao P, Li L, Jiang X, et al. Mismatch repair deficiency/microsatellite instability-high as a predictor for anti-PD-1/PD-L1 immunotherapy efficacy. *J Hematol Oncol*. 2019;12(1):54. doi:10.1186/s13045-019-0738-1
100. Rakesh R, PriyaDharshini LC, Sakthivel KM, Rasmi RR. Role and regulation of autophagy in cancer. *Biochimica et Biophysica Acta*. 2022;1868(7):166400.
101. Kwon J, Bakhoum SF. The Cytosolic DNA-Sensing cGAS-STING Pathway in Cancer. *Cancer Discov*. 2020;10(1):26–39. doi:10.1158/2159-8290.CD-19-0761
102. Lin H, Yan J, Wang Z, et al. Loss of immunity-supported senescence enhances susceptibility to hepatocellular carcinogenesis and progression in Toll-like receptor 2-deficient mice. *Hepatology*. 2013;57(1):171–182. doi:10.1002/hep.25991
103. Peng G, Guo Z, Kiniwa Y, et al. Toll-like receptor 8-mediated reversal of CD4 + regulatory T cell function. *Science*. 2005;309(5739):1380–1384. doi:10.1126/science.1113401
104. Wang Q, Wang P, Xiao Z. Resistant starch prevents tumorigenesis of dimethylhydrazine-induced colon tumors via regulation of an ER stress-mediated mitochondrial apoptosis pathway. *Int J Mol Med*. 2018;41(4):1887–1898. doi:10.3892/ijmm.2018.3423
105. Kang Y, Jiang X, Qin D, et al. Efficacy and safety of multiple dosages of fostamatinib in adult patients with rheumatoid arthritis: a systematic review and meta-analysis. *Front Pharmacol*. 2019;10:897. doi:10.3389/fphar.2019.00897
106. Skinner M, Philp K, Lengel D, et al. The contribution of VEGF signalling to fostamatinib-induced blood pressure elevation. *Br J Pharmacol*. 2014;171(9):2308–2320. doi:10.1111/bph.12559
107. Montero JC, Seoane S, Ocaña A, et al. Inhibition of Src family kinases and receptor tyrosine kinases by dasatinib: possible combinations in solid tumors. *Clin Cancer Res*. 2011;17(17):5546–5552. doi:10.1158/1078-0432.CCR-10-2616
108. Motzer RJ, Nosov D, Eisen T, et al. Tivozanib versus sorafenib as initial targeted therapy for patients with metastatic renal cell carcinoma: results from a Phase III trial. *J Clin oncol*. 2013;31(30):3791. doi:10.1200/JCO.2012.47.4940
109. Rini BI, Pal SK, Escudier BJ, et al. Tivozanib versus sorafenib in patients with advanced renal cell carcinoma (TIVO-3): a Phase 3, multicentre, randomised, controlled, open-label study. *Lancet Oncol*. 2020;21(1):95–104. doi:10.1016/S1470-2045(19)30735-1
110. Fischer T, Stone RM, DeAngelo DJ, et al. Phase IIB trial of oral Midostaurin (PKC412), the FMS-like tyrosine kinase 3 receptor (FLT3) and multi-targeted kinase inhibitor, in patients with acute myeloid leukemia and high-risk myelodysplastic syndrome with either wild-type or mutated FLT3. *J Clin Oncol*. 2010;28(28):4339–4345. doi:10.1200/JCO.2010.28.9678
111. El Fitori J, Su Y, Büchler P, et al. PKC 412 small-molecule tyrosine kinase inhibitor: single-compound therapy for pancreatic cancer. *Cancer*. 2007;110(7):1457–1468. doi:10.1002/cncr.22931
112. Mirza Z, Schulten H-J, Farsi HM, et al. Molecular interaction of a kinase inhibitor midostaurin with anticancer drug targets, S100A8 and EGFR: transcriptional profiling and molecular docking study for kidney cancer therapeutics. *PLoS One*. 2015;10(3):e0119765. doi:10.1371/journal.pone.0119765
113. Corsetti M, Landes S, Lange R. Bisacodyl: a review of pharmacology and clinical evidence to guide use in clinical practice in patients with constipation. *Neurogastroenterol Motil*. 2021;33(10):e14123. doi:10.1111/nmo.14123
114. Morrison BL, Mullendore ME, Stockwin LH, et al. Oxyphenisatin acetate (NSC 59687) triggers a cell starvation response leading to autophagy, mitochondrial dysfunction, and autocrine TNF α-mediated apoptosis. *Cancer Med*. 2013;2(5):687–700. doi:10.1002/cam4.107

115. Teh LB, Chong R, Ho JM, et al. Oxyphenisatin induced chronic active hepatitis--a potential health hazard in Singapore. *Singapore Med J*. 1988;29(5):508–512.
116. Matsukawa N, Grzesik WJ, Takahashi N, et al. The natriuretic peptide clearance receptor locally modulates the physiological effects of the natriuretic peptide system. *Proc Natl Acad Sci U S A*. 1999;96(13):7403–7408. doi:10.1073/pnas.96.13.7403
117. Sun A, Sheng X, Tang J, et al. Integrated bioinformatics and experimental approaches identified the role of NPPA in the proliferation and the malignant behavior of breast cancer. *J Immunol Res*. 2021;2021:7876489. doi:10.1155/2021/7876489
118. Nomiri S, Hoshyar R, Chamani E, et al. Prediction and validation of GUCA2B as the hub-gene in colorectal cancer based on co-expression network analysis: in-silico and in-vivo study. *Biomed Pharmacother*. 2022;147:112691. doi:10.1016/j.biopha.2022.112691